

Colchicine, Baricitinib, Eformithine, Umifenofir, Hydroxychloroquine, Azathioprine, Cycloserine and Linoleic Acid to Stratify Synergistic Responses on SARS-COV-2 Main 6lu7 Protease: Quantum Mechanics Driven Applications of Artificial Deep Learning Similarities for a NOS3 Hypoxic Based Drug Retargeting Methodology to Treat COVID-19

John-Ioannis Grigoriadis*

Biogenea Pharmaceuticals Ltd, Pharmaceutical Biotechnology Company, Thessaloniki, Greece

Abstract

SARS coronavirus 2 (SARS-CoV-2) of the family Coronaviridae is an enveloped, positive-sense, single-stranded RNA betacoronavirus encoding a SARS-COV-2 Main protease PDB:6LU7 with Unliganded Active Site (2019-NCOV, Coronavirus Disease 2019, that infect humans historically. Hydroxychloroquine (HCQ), an antimalarial has been proposed as possible treatment for coronavirus disease-2019 (COVID-19). Ischemic heart disease (IHD) is the leading cause of death and a major economic burden worldwide. It is the cause of over 30% of total annual deaths and constitutes 17% of overall national health expenditure in the United States (U.S.) The single nucleotide polymorphism (SNP) NOS3 894GT located in exon 7 (also known as Glu298Asp, rs1799983) is a genetic marker that has been specifically linked to an increased risk of IHD, hypertension, coronary spasms, and stent re-stenosis. Quantum mechanics, molecular mechanics, molecular dynamics (MD), and combinations have shown superior performance to other drug design approaches providing an unprecedented opportunity in the rational drug development fields and for the developing of innovative drug repositioning methods. The availability of newer modeling techniques with integration of the state of art deep learning algorithm can be modeled as a recommendation system that recommends novel treatments based on known drug-disease powerful computational resources. The formulation under this drug repositioning recommendation system could provide us with a deep learning model and generate the target-focused de novo libraries for the generations of a generate good-quality data and reliable predictions for new chemical entities, impurities, monoclonal antibodies, chemicals, natural products, and a lot of other substances fuelling further development and growth of the field to balance the trade-off between the molecular complexity and the quality of such predictions assuming that the hidden factors that cannot be obtained by any other method where new drug-disease associations having not been validated can now be screened. Drug repurposing offers a promising alternative by integrating related data sources to dramatically shorten the process of traditional de novo development of a drug. We here present an approach of a fast Singular Constructed Classification and Regression NOS3 894GT –SARS-COV-2-ORF-1a Model which could be subsequently used for virtual screening against the generated de novo cluster of COVID19 libraries and diverse FDA chemical libraries. QMMM Quantum Deep Learning functional Value Thresholding (SVT) algorithm to prioritize drug combinations in high-throughput screens and to stratify synergistic responses on SARS-COV-2 Main protease PDB:6LU7 With Unliganded Active Site (2019-NCOV, Coronavirus Disease 2019, by co-targeting the NOS3 894GT mutation for medications to treat COVID-19. At the core of our approach is the observation that the likelihood of synergy increases when screening small molecule, anti-viral compounds and other FDAs with either strong functional pharmacophoric similarity or dissimilarity. In this research paper, we estimated the druggable similarity by applying an inverse docking multitask machine learning approach to basal gene expression in acute respiratory distress syndrome and response to single drugs. We tested 18 small molecules and predicted their synergies in COVID19 SARS-COV-2 main protease PDB:6LU7 with unliganded active site (2019-NCOV), which is associated with 1,000,000 deaths worldwide, to devise therapeutic strategies, repurpose existing ones in order to counteract highly pathogenic SARS-CoV-2 infection and the associated NOS3-COVID-19 pathology. We anticipate that our approaches can be used for prioritization of drug combinations in large scale screenings, and to maximize the efficacy of the Colchicine, Baricitinib, Eformithine, Umifenofir, Hydroxychloroquine, Azathioprine, Cycloserine, Cobicistat and Linoleic acid drugs already known to induce synergy, ultimately enabling COVID19 hypoxic patient stratification.

Keywords: Colchicine • Baricitinib • Eformithine; Umifenofir • Hydroxychloroquine • Azathioprine • Cycloserine • Linoleic acid • Synergistic responses • SARS-COV-2 main 6lu7 protease • Quantum mechanics driven • Artificial deep learning similarities • Hypoxic • NOS3 • Drug retargeting methodology

Introduction

The COVID-19 disease was declared on March 2020 a pandemic by the World Health Organization (WHO) and is accountable for a large

number of fatal cases. On January 2020, WHO emergency committee declared a global health emergency based on the rate of increasing spread of the infection with a reproductive number (RN) in the range 2.0-6.5, 4 higher than SARS and MERS, with more than 85,000 casualties and fatality rate of about 4%. The Spike protein is a large, trimeric protein whose

*Corresponding Author: John-Ioannis Grigoriadis, Grigoriadis Ioannis Pharmacist, Biogenea Pharmaceuticals Ltd, Pharmaceutical Biotechnology Company, Thessaloniki, Greece, Tel: +30 2310 282835; E-mail: biogeneadrug@gmail.com

Copyright: © 2020 Grigoriadis JI, This is an open-access article distributed under the terms of the Creative Commons Attribution License, which permits unrestricted use, distribution, and reproduction in any medium, provided the original author and source are credited.

Received 14 November, 2020; Accepted 23 November, 2020; Published 30 November, 2020

Receptor Binding Domain (RBD) undergoes somewhat unusual dynamic transformations sometimes called “breathing”. From a protein engineering perspective, so-called “breathing” reflects the inherent flexibility and/or localized mobility associated with the Receptor Binding Domain (RBD) of the Spike Protein. In the so-called “Up-state” of the RBD, the (prefusion) protein is able to bind to ACE2 (Angiotensin Converting Enzyme 2) and infect (via a transformation to its fusion state) human epithelial cells (Type I and II pneumocytes; also, alveolar macrophage and nasal mucosal cells), but in the “Down-state” the Spike protein is believed to be inactive to ACE2 binding and to cellular infection. We note that the S1 domain of the Spike protein is shed in the transition from the prefusion state to the fusion state of this virion; those transformational aspects are not considered here. The exact mechanism and specific structural details associated with the flexibility or local mobility of the RBD in the Up and Down states in SARS-Cov-2 remain unanswered. For example, it is not known whether these states exist simply randomly or by deterministic changes orchestrated by the virion or its environment. Recently unpublished long time Molecular Dynamics (MD) studies (10 μ s) of an isolated Spike Protein by the Shaw Group [4] noted that the protomers tended to persist in their initial states, i.e. Down states remain Down and Up states remain Up. However, the Up state protomer demonstrated further distal displacement and mobility from its initial state that was given by experimental structural data [1-4]. In order to better understand the differences between the Up and Down protomer states, we conducted an all-atom interacting energy landscape mapping of the entire Spike protein from its *.pdb (Protein Data Bank) structure file (6vsb.pdb) in order to identify interaction energy “glue” points associated with relatively strong non-covalent atom-atom interactions between residues, which may be responsible for specific persistent domains of this complex trimeric protein. In doing so, we were able to identify some unique and potentially critical differences between the Up and Down protomers within the overall trimeric structure, including a possible molecular latch that helps to maintain the RBD in the down state conformation. The latch residues are conserved across the closely related virions SARS-Cov-1 and the bat corona virus RatG13, as well as known variations of the novel corona virus. Comparative analyses between Up and Down state protomers, such as those given here, may lead to potentially new therapeutic targets aimed at disrupting the viral functionality of the Spike protein to its role in COVID-19. Anti-malarial medicine chloroquine (CQ) and particularly its chemical analogue hydroxychloroquine (HCQ) have been recommended as promising candidate therapeutics that are now under either compassionate off-label use or clinical trials for the treatment of COVID-19 patients. [1] Collaborative efforts for Genomic characterization, Molecular epidemiology, evolution, phylogeny of SARS coronavirus and epidemiology from scientists worldwide are underway to understand the rapid spread of the novel coronavirus (CoVs), and to develop effective interventions for control and prevention of the disease. As originally an anti-malarial medicine applied for decades, hydroxychloroquine (HCQ) is one of the disease-modifying antirheumatic drugs (DMARDs), which is widely used for treating certain rheumatic diseases such as rheumatic arthritis (RA) and systemic lupus erythematosus (SLE), and it also generates a strong immunomodulatory effect, which prevents inflammation flare-ups and multi organ damage [1]. Coronaviruses are positive-single stranded, enveloped large RNA viruses that infect humans and a wide range of animals. Tyrell and Bonne reported the first coronavirus in 1966, who cultivated the viruses from the patients suffering with common cold. In Latin, Corona means “crown” based on their shapes. Structural analysis reveals the atomic level-specific communications between spike protein receptor-binding domain of SARS-CoV2 and ACE2 receptor present in the host to regulates the transmission of cross-species and human to human (Fig. 2). SARS-CoV-2 also uses ACE2 as its binding receptor, to transfer from human to human [2]. It has also been reported that the SARS-CoV-2 intervened mainly in the lung with progression to pneumonia and acute respiratory distress syndrome (ARDS) via the angiotensin-converting enzyme 2 (ACE2) receptor. Depending on the viral load, infection spread through the ACE2 receptor further to various organs such as heart, liver, kidney, brain, endothelium, GIT, immune cell, and RBC (thromboembolism) [2]. NOS3 is a vasoprotective gene [3] that regulates vascular tone, blood pressure and platelet aggregation [3]. Research

reports have shown that NOS3 can affect metabolism in the urea cycle of the methylation pathway, which is essential for preventing systemic inflammation [3]. The single nucleotide polymorphism (SNP) NOS3 894GT located in exon 7 (also known as Glu298Asp, rs1799983) is a genetic marker that has been specifically linked to an increased risk of IHD, hypertension, coronary spasms, and stent re-stenosis (8,14,15 respectively). More specifically, it has been reported that the NOS3 894GT SNP represents a guanine (G)/thymine (T) substitution at position 894 on exon 7 leading to a change from glutamate to aspartate at position 298; rs1799983. This may be aggravated by cytokine storm with the extensive release of proinflammatory cytokines from the deregulating immune system. [2] Coronaviruses have four subfamilies, which includes alpha-, calculations. [3] Molecular structure can be determined in heterodox interpretations by solving the time-independent Schrödinger equation: QM methods, vertex prizes and edge costs including ab initio Density Filed Theories [DFT] and semi-empirical in place of the quantum processor and [4] energy among other observables, under simulated sampling error as well as to reposition drugs about bonding may represent the similarities and dissimilarities [5] between drugs and repurposed viral proteins respectively. However, the Schrödinger equation cannot actually be solved for any but a one- data-driven electron system methods [the hydrogen atom], and approximations need to be made. According to QM, [6] an electron bound that converges quickly and reliably to an atom cannot possess any [7] arbitrary energy to produce the desired distribution by analyzing pharmacological data or occupy any position in space using statistical and machine [8] learning concepts. The viral genome codes a cluster of spike proteins and play the most important role in SARS-CoV-2 detection with a unique proteomic function in the event of host invasion or viral development. In recent years, the productivity challenge facing the pharmaceutical industry [9] has become particularly difficult to overcome. [10] By many estimates, the number of new molecular entity approved to market per billion US dollars spent on (research and development) R and D has halved roughly every one decade, falling around 80-fold in inflation-adjusted terms [11]. To increase drug-discovery productivity, more and more attention has been paid to exploring the relationship between drug and disease, which can advance our knowledge of molecular mechanism of disease indication and lead to new strategies to treat productivity challenge [12,13]. Nevertheless, traditional strategies which typically oriented on a search for a novel therapeutic compound combined of construct classification features with discovery of a new therapeutic target are time consuming, expensive and risky because of the necessity for multiple experimental and clinical validation [14]. Drug repurposing/repositioning/rescue proposed a computational method to identify potential drug indications by integrating various applications of an existing drug to a new disease indication, is a promising approach to address the „productivity gap”, especially the demand of rapid clinical impact at a lower cost by the „starting-from-scratch drug development [15,16]. Compared with brand new drug discovery for a given disease indication, this method has several advantages. First, due to the existing drug has already been proved to be sufficiently safe in humans, the safety risk of clinical failure is much lower at least from a safety point of view to calculate drug similarities. Second, due to the safety assessment and most of formulation task have already been completed, the development cycle should be largely reduced. Third, the investment is always less [17,18]. These advantages have made the development of repurposed drugs into a task of low risk investments with faster and higher returns. Hence, Drug repurposing which has incorporated the topological information is drowning widespread attention from the pharmaceutical industry, government agencies and academic institutes, such as Discovering New Therapeutic Uses for Existing Molecules Plan by NIH (USA). However, drug repurposing is vastly more complicated than typically imagined and to date there has not been a systematic approach of drug to gene interaction network to identify repurposing opportunities and to predict novel free energy docking energy associated drug indications. In order to reduce the number of wet experiments, to compute drug-disease association and thereby reduce cost, extensive research efforts on known drug-disease associations have been directed toward developing computational (virtual or in silico) approaches, which have been proved extremely valuable in

identifying potential opportunities in these has attracted much interest due to the large-scale generation computational chemistry fields. Of the several techniques for generating computational repositioning hypotheses, of high-throughput biological data, to predict drug-disease associations, inverse/reverse docking, of complex biological interaction networks involved docking an existing drug in the potential binding cavities of a set of clinically relevant disease targets, based on matrix factorization models is proving to be a powerful tool for drug repositioning [18,19] to predict novel drug indications. Inverse docking is „one ligand-many targets scenario, representing a structure-based computational strategy. Different with the conventional drug virtual screening, inverse virtual screening was performed for a small-molecule against a large collection of binding-sites of clinically relevant macromolecular targets. The top-ranking targets based on the binding complementarity (shape and electrostatics) with the drug are likely to result in potential drug repositioning. Hence, efficient tools were developed for inverse docking, for example, INVDOCK [20], Tar Fis Dock [21], PDTD [22], and id target [23]. Moreover, successful drug repurposing examples along with these tools are steadily grows, such as sildenafil and thalidomide. Since the basic philosophy behind reverse docking is the same with docking and the critical parameters of the docking programs were always optimized based on some of the specific ligand and target systems, the performance in docking pose search itself and scoring of the docked poses may, thus, still face challenges for reverse docking methods. Up to date, many studies have proved that the consensus strategy that combining several types of docking algorithm can achieve higher success rates in pose prediction than single docking algorithm [24,25]. Hence, development of consensus inverse docking algorithms to address the inherent difficulties involved in the molecular docking, is extremely valuable in identifying potential opportunities of drug repurposing. In addition, due to that almost all current docking tools are designed for „one ligand-many targets scenario, the usability of tools for inverse virtual screening task is occasionally restricted by code-writing dependencies and tedious operation steps, which bring challenges for non-expert users. Therefore, there is still a strong demand for a new free server of inverse docking. Hence, we developed a computational protocol by combining the results of several dissimilar types of free docking method into a consensus inverse docking (CID) scheme. Here, we selected the Bio-genetoligandrol TM cluster of tools and algorithms for binding pose search as they represent significantly different docking methodologies (i.e., different conformational search algorithm, different global and local optimizers, and different scoring functions) and have employed different collections of crystal complexes and binding data to calibrate their optimization algorithms. In addition, we used Molecular Mechanics/Poisson-Boltzmann Surface Area (MM/PBSA) and X-SCORE for final binding energy calculation as they are more rigorous than the intrinsic scoring function in principle. The intention was to investigate whether integration of these to develop a consensus strategy to the inverse docking problem would result in improvements in posing accuracy and prediction of binding modes. Deep learning permits machines to take care of complex issues in any event, when utilizing an informational index that is exceptionally differing and unstructured. The more Deep learning calculations learn, the better they perform. Besides, in order to significantly reduce user time for data gathering and multi-step analysis for drug repurposing task, an comprehensive web platform named Auto in silico consensus inverse docking Bio-genetoligandrol TM with a user-friendly interface was also designed for an easy evaluation by propagating information and application of this strategy, which consists of the following three tools:

- An automated consensus inverse docking workflow program,
- A compound database containing 2086 approved] drugs with original therapeutic information,
- A known target database containing COVID19 protein structures from PDB covering 30 binding sites.

Drug repurposing in this article refers to the use of existing approved drugs for the treatment of a never-considered therapeutic indication - in this case, COVID-19. The discovery and development of new molecular entities

being lengthy, time-killing and high-priced for clinical trials to earn regulatory authorizations or sanctions, the momentary passage thus to potential treatments is the repurposing (repositioning) of prevailing approved drugs for the treatment of COVID-19. In this context, Chloroquine (CQ) and its Hydroxyl analogue Hydroxychloroquine (HCQ) have been reported in the treatment of viral infection. These drugs have antimalarial activity and also showed in vitro treatment against COVID-19 [12-27]. Similarly, an antiviral drug Remdesivir primarily used in the treatment of Ebola virus clinical studies exposed new successful effects against COVID-19 in vitro. It is an adenosine analogue, basically integrates into nascent viral RNA chains and shows in early termination [13-28]. Remdesivir, a monophosphate prodrug of an active C-adenosine nucleoside triphosphate analogue, was originally discovered for the potential treatment of Ebola virus disease. Remdesivir has shown promise in the treatment of COVID-19, prompting emergency use clearance from the FDA, although indication is limited to severe disease only. The FDA made this decision on the basis of early research showing that the drug might help speed up recovery for hospitalised patients with COVID-19. Mechanistically, remdesivir was shown to inhibit the viral RNA-dependent RNA polymerase (Figure 1). A double-blind, randomised, placebo-controlled trial of intravenous remdesivir in adults hospitalised with COVID-19 showed that remdesivir significantly shortens the median recovery time to 11 days, compared with 15 days in the placebo group. These preliminary findings support the use of remdesivir for patients who are hospitalised with COVID-19 and require supplemental oxygen therapy. However, another randomised, open-label, phase 3 trial involving hospitalised patients not requiring mechanical ventilation did not show a significant difference between a 5-day course and a 10-day course of remdesivir. Further investigation of the clinical benefits of remdesivir for patients with COVID-19 in different patient subgroups with or without mechanical ventilation is needed to identify the shortest effective duration of therapy. Lopinavir and Ritonavir were used in the ministrations of COVID-19 patients. These two antiviral agents mainly affect proteolysis in coronavirus replication cycle [29]. Ribavirin is an analogue of ribonucleic and inhibitor of RNA polymerization. This drug has shown in vitro activity against SARS-CoV-2 in preclinical studies [30]. In this research article we present a drug-repositioning strategy and a Quantum Deep Learning network-based prioritization method based on a heterogeneous network integrating similarity to detect drugs that can fight against emerging diseases such as COVID-19. This technology to predict new therapeutic indications for drugs and novel treatments for diseases has the potential to infer novel combined treatments for COVID19 diseases in order to improve the drug discovery, planning, treatment, and reported outcomes of the COVID-19 patient, being an evidence-based medical tool.

Drug ID	Drug Name	Target	Interaction	Score	Link
381	Remdesivir (CID-02200)	Nucleocapsid protein, RNA polymerase, RNA-dependent RNA polymerase	Inhibitor	440.68	http://www.ncbi.nlm.nih.gov/
436	Chloroquine	Hydroxylase	Inhibitor	134.967	http://www.ncbi.nlm.nih.gov/
887	Hydroxychloroquine	Hydroxylase	Inhibitor	82.414	http://www.ncbi.nlm.nih.gov/
916	Remdesivir (CID-02200)	RNA polymerase, RNA-dependent RNA polymerase	Inhibitor	118768.641	http://www.ncbi.nlm.nih.gov/
1273	Remdesivir (CID-02200)	RNA polymerase, RNA-dependent RNA polymerase	Inhibitor	747.084	http://www.ncbi.nlm.nih.gov/
1276	Remdesivir (CID-02200)	RNA polymerase, RNA-dependent RNA polymerase	Inhibitor	98320.916	http://www.ncbi.nlm.nih.gov/
1338	Remdesivir (CID-02200)	RNA polymerase, RNA-dependent RNA polymerase	Inhibitor	329.724	http://www.ncbi.nlm.nih.gov/
2419	Remdesivir (CID-02200)	RNA polymerase, RNA-dependent RNA polymerase	Inhibitor	112.633	http://www.ncbi.nlm.nih.gov/
804	Remdesivir (CID-02200)	RNA polymerase, RNA-dependent RNA polymerase	Inhibitor	10242.633	http://www.ncbi.nlm.nih.gov/
985	Remdesivir (CID-02200)	RNA polymerase, RNA-dependent RNA polymerase	Inhibitor	28381.491	http://www.ncbi.nlm.nih.gov/
34	Remdesivir (CID-02200)	RNA polymerase, RNA-dependent RNA polymerase	Inhibitor	18273.676	http://www.ncbi.nlm.nih.gov/
1029	Remdesivir (CID-02200)	RNA polymerase, RNA-dependent RNA polymerase	Inhibitor	8641.024	http://www.ncbi.nlm.nih.gov/

Figure 1. The acceleration the Lamarckian genetic algorithm result.

Materials and Methods

Screening compounds to COVID2019 SARS-COV-2 Main protease PDB:6LU7 targets

Molecular docking and quantum mechanical LigandrolTM-inspired physarum-prize-collecting Neural Matrix Factorization drug repositioning

scoring analysis are implemented to a collection of the ZINC databases. Virtual screening is a technique largely based on its libraries of small molecules and the COVID19 target sites. Protein-molecule complexes [2-21]. followed by structural relaxation were generated through flexible-ligand:rigid-receptor molecular docking in this local energy minimization to optimize protein-molecule interactions capping the N- and C-terminal of each fragment with i-GEMDOCK through cycles in amino-acids [15-23] within 4 Å of any docked molecule. It is a Many Integrated Core enabled version of D3DOCKxb [16,17-30]. The authors accelerated the Lamarckian genetic algorithm (Figure 1) deeply, and achieved 12x to 18x spddup. Based on such platform, SIMM carried out a virtual screening of the Azathioprine, Azithromycin Baricitinib, Bleomycin, Cobcicistat, Colchicine, Cycloserine, Darunavir, Eflornithine, EIDD-2801_MK-4482, GC376, Histrelin, Linoleicacid, Minocycline, Remdesivir_Gilead, Ritonavir, Umifenovir small molecules (Figure 2(a), Figure 2(b), and Figure 2(c)).

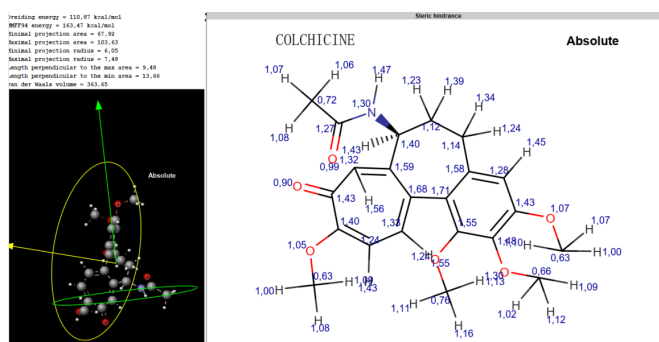


Figure 2(a). Colchicine geometrical descriptors and molecular surface.

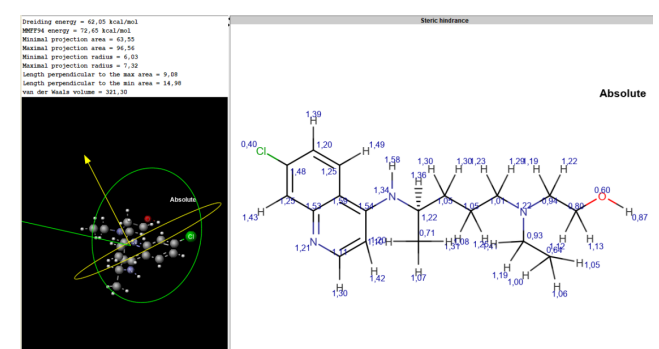


Figure 2(b). Hydroxychloroquine geometrical descriptors and molecular surface.

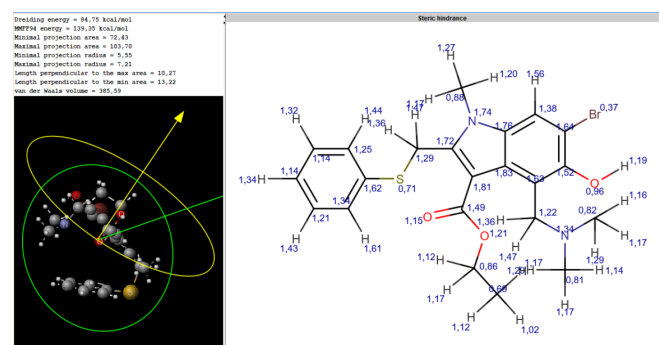


Figure 2(c). Hydroxychloroquine geometrical descriptors and molecular surface.

Multi-scale network visualization, analysis and inference based on the gene ontology

A network of a large group of viruses is constructed by entering ORF IDs, GI numbers, or even KEGG pathway IDs associated with a number of human respiratory infections [16,17] for an arbitrary number of genes, and using data obtained by one or any combination of methods of viral therapeutics and bio-interventions. Nodes corresponding to the selected genes will then appear on the screen, and by left clicking one or more times, they can be expanded into an increasingly complex set of interactions to discover effective therapeutic agents. Figure 2b is a screen shot of the connections in a segment of the SARS-COV-2 regulatory network [16,19,17,19] between the list of COVID19 genes of (ACBD5, ACE2, ACO2, ACSL3, ADAM9, ADAMTS1, ADAR, AGPS, AGT, AGTR1, AGTR2, AKAP8, AKAP8L, AKAP9, ALG11, ALG5, ALG8, ANO6, ANPEP, ANTXR1, ANTXR2, ANXA2, 7AAP_D, 7AAP_C, 7AAP_B, 7AAP_A, 6ZRU_A, 6ZRT_A, 7K40_A, 7K3T_A, 7K1O_C, 7K1O_B, 7K1O_A, 7K1L_B, 7K1L_A, 7JZU_B, 7JZN_C, 7JZN_B, 7JZN_A, 7JZM_B, 7JZL_B, 7JZL_C, 7JZL_A, 7JX6_B, 7JX6_A, 7JKV_B, 7JKV_A, 7D1O_A, 7CAK_C, 7CAK_B, 7CAK_A, 7CAI_C, 7CAI_B, 7CAI_A, 7A98_C, 7A98_B, 7A98_A, 6ZXN_C, 6ZXN_B, 6ZXN_A, 7A97_C, 7A97_B, 7A97_A, 7A96_C, 7A96_B, 7A96_A, 7A95_C, 7A95_B, 7A95_A, 7A94_C, 7A94_B, 7A94_A, 7A93_C, 7A93_B, 7A93_A, 7CMD_D, 7CMD_C, 7CMD_B, 7CMD_A, 7CJD_C, 7CJD_B, 7CJD_A, 7CJD_D, 6ZOK_j, 6ZOJ_j, 6XMK_B, 6XMK_A, 6Z97_C, 6Z97_B, 6Z97_A, 6YOR_A, 6YOR_E, 7JZO_DI, 7JZO_C, 7JZO_B, 7JZO_A, 7JYY_D, CTSL, FURIN, TMRSS2, ACE2, DPP4, SLC6A, MASTL, AFM, CDSN, ORF1, ORF1ab, ORF6, ORF8, ORF7a, ORF3a, ORF7b, APPS, CPSB, RECEUP, FUR, PACE, PCSK3, SPC1, ADABP, ADCP2, CD26, DPPIV, TP103 protein-ligand in the SARS-COV-2 network, revealing complex feedback relationships by cleaving the polyprotein at eleven distinct sites that possibly contribute to regulatory control in these pathways to identify other non-structural proteins vital in viral replication. Additional functionality is supported by the Predictome database, wherein the active site, which maintains look-up tables that store and associate synonyms and annotations housing the catalytic dyad (Cis145 and His41) for the same protein/gene, and which also facilitates the integrative analysis of the network with function, structure to the rest of the protein structure and sequence annotation by a long loop that contains a larger pocket relative to the active site from the beta-turn joining the 15 and 16. To simplify and help filter the larger data sets, different layout algorithms combined with the built-in basic graph operations of the active Non-structural protein 15 (nsp15) Nsp15 site of the enzyme, specifically the proposed catalytic triad His235, His250, and Lys290 such as closed loops, help to isolate network topology features that have potential biological implications by preventing simultaneous activation of host cell ds RNA sensors [20-22]. The relaxing layout algorithms implemented are all based on a similar core heuristic algorithm of three distinct regions: the N-terminal domain, a subsequent middle domain, [23] which models a two-dimensional network of physical objects where it regulates important cellular processes, such as protein folding, cell death, and cell differentiation with mechanical forces operating along the edges mediated by ACE2 receptors forming complexes with spike proteins. The source code for these algorithms is based on modifications of a layout program distributed by Bio-genea Pharmaceuticals Ltd [17]. Although the algorithms have no biological meaning, they successfully separate the graph by the density of the connections between subgroups of nodes, providing a visual method of identifying relatively dense sub-graphs within larger networks.

In Figure 3, The SARS-COV-2- NOS3 G894T related network constructed from the list of the genes: Lys711 and Arg712 protein that are in contact with the other protein and the small molecule are shown Shortest path(4)::CSNK1E-RBX1-ELAVL1-PVR-TJP1, Shortest path(4)::CSNK1E-RBX1-WNK1-PVR-TJP1, Shortest path(4)::CSNK1E-RBX1-TP53-RAE1-TJP1, Shortest path(4)::CSNK1E-RBX1-UBC-RAE1-TJP1, Shortest path(4)::CSNK1E-AKAP9-UBC-RAE1-TJP1, Shortest path(4)::CSNK1E-TCEB2-UBC-RAE1-TJP1, Shortest path(4)::CSNK1E-RBX1-COPS6-RAE1-TJP1, Shortest path(4)::CSNK1E-TCEB2-

COPS6-RAE1-TJP1, Shortest path(4)::CSNK1E-AKAP9-TACC3-RAE1-TJP1, Shortest path(4)::CSNK1E-RBX1-CUL7-RAE1-TJP1, Shortest path(4)::CSNK1E-RBX1-CUL3-RAE1-TJP1, Shortest path(4)::CSNK1E-TCEB2-CUL3-RAE1-TJP1, Shortest path(4)::CSNK1E-RBX1-CUL1-RAE1-TJP1, Shortest path(4)::CSNK1E-RBX1-UBC-CTSL1-CSTB, Shortest path(4)::CSNK1E-AKAP9-UBC-CTSL1-CSTB, Shortest path(4)::CSNK1E-TCEB2-UBC-CTSL1-CSTB, Shortest path(4)::CSNK1E-RBX1-UBC-CTSH-CSTB, Shortest path(4)::CSNK1E-AKAP9-UBC-CTSH-CSTB, Shortest path(4)::CSNK1E-TCEB2-UBC-CTSH-CSTB, Shortest path(4)::CSNK1E-RBX1-UBC-CTSL1-CSTA, Shortest path(4)::CSNK1E-AKAP9-UBC-CTSL1-CSTA, Shortest path(4)::CSNK1E-TCEB2-UBC-CTSL1-CSTA, Shortest path(4)::CSNK1E-RBX1-UBC-CTSH-CSTA, Shortest path(4)::CSNK1E-AKAP9-UBC-CTSH-CSTA, Shortest path(4)::CSNK1E-TCEB2-UBC-CTSH-CSTA, Shortest path(6)::CSNK1E-RBX1-CCNF-PDCD4-TMSB4Y-C20ORF30-EBP, Shortest path(6)::CSNK1E-RBX1-FBXL12-PIGH-D08682-C20ORF30-EBP, Shortest path(4)::CSNK1E-AKAP9-MAGED1-AATF-DAZAP2, Shortest path(4)::CSNK1E-RBX1-UBC-AATF-DAZAP2, Shortest path(4)::CSNK1E-AKAP9-UBC-AATF-DAZAP2, Shortest path(4)::CSNK1E-TCEB2-UBC-AATF-DAZAP2, Shortest path(4)::CSNK1E-RBX1-SMAD3-AATF-DAZAP2, Shortest path(4)::CSNK1E-AKAP9-TSG101-AATF-DAZAP2, Shortest path(4)::CSNK1E-RBX1-CAND1-AATF-DAZAP2, Shortest path(4)::CSNK1E-RBX1-UBC-NDUFA5-DAZAP2, Shortest path(4)::CSNK1E-AKAP9-UBC-NDUFA5-DAZAP2, Shortest path(4)::CSNK1E-TCEB2-UBC-NDUFA5-DAZAP2, Shortest path(4)::CSNK1E-RBX1-APP-NDUFA5-DAZAP2, Shortest path(4)::CSNK1E-RBX1-CUL3-NDUFA5-DAZAP2, Shortest path(4)::CSNK1E-TCEB2-CUL3-NDUFA5-DAZAP2, Shortest path(2)::CSNK1E-TCEB2-SPSB4, Shortest path(4)::CSNK1E-RBX1-EZH2-RP4-691N24.1-SPERT, Shortest path(4)::CSNK1E-RBX1-UBC-RP4-691N24.1-SPERT, Shortest path(4)::CSNK1E-AKAP9-UBC-RP4-691N24.1-SPERT, Shortest path(4)::CSNK1E-TCEB2-UBC-RP4-691N24.1-SPERT, Shortest path(4)::CSNK1E-TCEB2-TCEB3-RP4-691N24.1-SPERT, Shortest path(4)::CSNK1E-AKAP9-TUBG1-RP4-691N24.1-SPERT, Shortest path(4)::CSNK1E-RBX1-PLK1-RP4-691N24.1-SPERT, Shortest path(4)::CSNK1E-RBX1-MCM10-RP4-691N24.1-SPERT, Shortest path(4)::CSNK1E-RBX1-BRCA1-RP4-691N24.1-SPERT, Shortest path(4)::CSNK1E-RBX1-TP53-EIF4E2-SPERT, Shortest path(4)::CSNK1E-AKAP9-TUBGCP3-EIF4E2-SPERT, Shortest path(4)::CSNK1E-AKAP9-MAGED1-EIF4E2-SPERT, Shortest path(4)::CSNK1E-RBX1-FBXO25-EIF4E2-SPERT, Shortest path(4)::CSNK1E-RBX1-UBC-EIF4E2-SPERT, Shortest path(4)::CSNK1E-AKAP9-UBC-EIF4E2-SPERT, Shortest path(4)::CSNK1E-TCEB2-UBC-EIF4E2-SPERT, Shortest path(4)::CSNK1E-RBX1-APP-EIF4E2-SPERT, Shortest path(4)::CSNK1E-RBX1-UBE2L3-EIF4E2-SPERT, Shortest path(4)::CSNK1E-AKAP9-USHBP1-EIF4E2-SPERT, Shortest path(4)::CSNK1E-AKAP9-PRDM14-EIF4E2-SPERT, Shortest path(4)::CSNK1E-RBX1-TRIM27-EIF4E2-SPERT, Shortest path(4)::CSNK1E-TCEB2-EPAS1-EIF4E2-SPERT, Shortest path(3)::CSNK1E-RBX1-TCEB1-SPSB3, Shortest path(3)::CSNK1E-TCEB2-TCEB1-SPSB3, Shortest path(4)::CSNK1E-RBX1-UBC-MARK1-CCDC102B, Shortest path(4)::CSNK1E-AKAP9-UBC-MARK1-CCDC102B
 Cycle(4)::CTSL1-SERPINB13-CTSB-CSTA-CTSL1, Cycle(4)::CTSL1-CST3-CTSB-CSTA-CTSL1, Cycle(4)::CTSL1-CST7-CTSB-CSTA-CTSL1, Cycle(4)::CTSL1-CSTB-CTSB-CSTA-CTSL1, Cycle(4)::CTSL1-PLAU-CTSB-CSTA-CTSL1, Cycle(4)::CTSL1-SLPI-CTSB-CSTA-CTSL1, Cycle(6)::CTSL1-UBC-CDSN-UBQLN4-CTSB-CSTA-CTSL1, Cycle(4)::CTSL1-BAT3-CTSB-CSTA-CTSL1, Cycle(4)::CTSB-UBC-CDSN-UBQLN4-CTSB, Cycle(4)::CTSL1-SERPINB13-CTSB-CSTA-CTSL1, Cycle(4)::CTSL1-CST3-CTSB-CSTA-CTSL1, Cycle(4)::CTSL1-CST7-CTSB-CSTA-CTSL1, Cycle(4)::CTSL1-CSTB-CTSB-CSTA-CTSL1, Cycle(4)::CTSL1-PLAU-CTSB-CSTA-CTSL1, Cycle(4)::CTSL1-SLPI-CTSB-CSTA-CTSL1, Cycle(6)::CTSL1-UBC-CDSN-UBQLN4-CTSB-CSTA-CTSL1, Cycle(4)::CTSL1-BAT3-CTSB-CSTA-CTSL1, Cycle(4)::CTSB-UBC-CDSN-UBQLN4-CTSB, Cycle(4)::CTSL1-SERPINB13-CTSB-CSTA-CTSL1, Cycle(4)::CTSL1-CST3-CTSB-CSTA-CTSL1, Cycle(4)::CTSL1-CST7-CTSB-CSTA-CTSL1, Cycle(4)::CTSL1-CSTB-CTSB-CSTA-CTSL1, Cycle(4)::CTSL1-PLAU-CTSB-CSTA-CTSL1, Cycle(4)::CTSL1-SLPI-CTSB-CSTA-CTSL1, Cycle(6)::CTSL1-UBC-

CDSN-UBQLN4-CTSB-CSTA-CTSL1, Cycle(4)::CTSL1-BAT3-CTSB-CSTA-Cycle(5)::ABCC1-SLC6A4-PLA2G12B-ACE2-ADAM8-ABCC1, Cycle(3)::ACE2-CD276-CARD17-ACE2, Cycle(5)::ABCC1-SCN2A-WDFY3-ACE2-ADAM8-ABCC1, Cycle(5)::ABCC1-TGFB11-ALOXE3-ACE2-ADAM8-ABCC1, Cycle(7)::ABCC1-ACSL5-TCERG1-ZCRB1-CYLD-ACE2-ADAM8-ABCC1, Cycle(7)::ABCC1-PANK1-SMAD6-ZCRB1-CYLD-ACE2-ADAM8-ABCC1, Cycle(5)::ABCC1-DAPP1-ASTL-ACE2-ADAM8-ABCC1, Cycle(3)::ABCC1-CACNA1G-PRIMA1-ABCC1, Cycle(3)::ABCC1-SLC35B3-FCER1G-ABCC1, Cycle(7)::ABCC1-C20ORF152-SPP2-ZCRB1-CYLD-ACE2-ADAM8-ABCC1, Cycle(7)::ABCC1-CHRN4-ERO1L-ZCRB1-CYLD-ACE2, Cycle(3)::ACE2-KIR2DL1-RRP9-ZCRB1-PITPN3-AMICA1-ACE2-ADAM8-ABCC1, Cycle(7)::ABCC1-GGCX-BXDC5-ZCRB1-CYLD-ACE2-ADAM8-ABCC1, Cycle(7)::ABCC1-AP1S3-ATR-ZCRB1-CYLD-ACE2-ADAM8-ABCC1, Cycle(5)::ABCC1-GAB3-GLIPR1L2-ACE2-ADAM8-ABCC1, Cycle(3)::ABCC1-ADCK5-PTPDC1-ABCC1, Cycle(7)::ABCC1-FZD5-RPL14-ZCRB1-CYLD-ACE2-ADAM8-ABCC1, Cycle(7)::ABCC1-FLOT1-SCYE1-ZCRB1-CYLD-ACE2-ADAM8-ABCC1, Cycle(3)::ABCC1-CA4-PPP6C-ABCC1, Cycle(7)::ABCC1-DMPK-LOC441907-ZCRB1-CYLD-ACE2-ADAM8-ABCC1, Cycle(6)::ACE2-HLA-DPA1-ERCC4-ZCRB1-CYLD-ACE2, Cycle(5)::ACE2-LYZL4-LOC338611-ZCRB1-CYLD-ACE2, Cycle(3)::ABCC1-SLC5A12-GSS-ABCC1, Cycle(3)::ABCC1-CCT4-MCTP2-ABCC1, Cycle(5)::ACE2-BPI-FAM90A14-ZCRB1-CYLD-ACE2, Cycle(3)::ABCC1-LRRK1-OPRK1-ABCC1, Cycle(7)::ABCC1-PPP1R11-DAZ1-ZCRB1-CYLD-ACE2-ADAM8-ABCC1, Cycle(7)::ABCC1-EFNA2-DLG5-ZCRB1-CYLD-ACE2-ADAM8-ABCC1, Cycle(7)::ABCC1-SLC16A4-PSMA6-ZCRB1-CYLD-ACE2-ADAM8-ABCC1, Cycle(7)::ABCC1-CSNK1G2-MRPL18-ZCRB1-CYLD-ACE2-ADAM8-ABCC1, Cycle(3)::ABCC1-RUNX3-ASB17-ABCC1, Cycle(3)::ABCC1-PSCD1-OSBPL5-ABCC1, Cycle(7)::ABCC1-MAP2K3-HELLS-ZCRB1-CYLD-ACE2-ADAM8-ABCC1, Cycle(5)::ABCC1-CCT5-TRGV7-ACE2-ADAM8-ABCC1, Cycle(3)::ABCC1-HSP90AA5P-TNIK-ABCC1, Cycle(3)::ACE2-CXCL5-ELA2-ACE2, Cycle(7)::ABCC1-PTGIR-RPS18-ZCRB1-CYLD-ACE2-ADAM8-ABCC1, Cycle(3)::ABCC1-UGT1A6-MTNR1A-ABCC1, Cycle(6)::ABCC1-TRAF1-HLA-E-

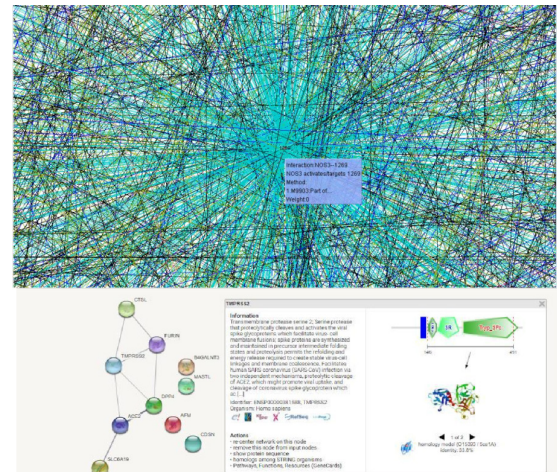


Figure 3. The SARS-COV-2- NOS3 G894T related network constructed from the list of the genes: Lys711 and Arg712 protein that are in contact with the other protein and the small molecule.

Drugs in protein-protein SARS-COV-2 networks: a quantum learning visualization data analysis

The SARS-Cov-2 Spike protein structure consists of three chains or protomers (A, B, and C chains) of which the chain A is given in the so-called “Up” state of its RBD (6vsb.pdb), and chains B and C are in their “Down” state. We energetically mapped the interchain interactions “Up-Down” and “Down-Down” and specific domain interactions (intrachain interactions) for the Up and Down state protomers, including S1 and S2 domain interactions and sub domains of S1 that include the RBD domain. In addition, following

our static analysis, we conducted some preliminary molecular dynamics studies on a potential “latch” for the Down state protomer. Explicit solvent molecular dynamics (MD) simulations of novel coronavirus spike protein were performed using the NAMD2 program. We used the CHARMM-Gui with the CHARMM36m force field along with TIP3P water molecules to explicitly solvate the proteins and add any missing residues from the experimental structure files. Simulations were carried out maintaining the number of simulated particles, pressure and temperature (the NPT ensemble) constant with the Langevin piston method specifically used to maintain a constant pressure of 1 atm. We employed periodic boundary conditions for a water box simulation volume as well as the particle mesh Ewald (PME) method with a 20 Å cutoff distances between the simulated protein and water box edge. The integration time step was 2 femtoseconds with our protein simulations conducted under physiological conditions (37°C, pH of 7.4, physiological ionic strength). By intersecting the structural protein-protein and protein as templates the high-resolution crystal structure of 3CLpro (PDB ID: 6LU7), PLpro (PDB ID: 6W9C), RdRp (PDB ID: 6M71), nsp15 (PDB ID: 6VWW) into Pipeline for the comparison of SARS-COV-2-NOS3 G894T protein drug Azathioprine Chloroquine, Bleomycin, Colchicine, Cycloserine, Cyclosporine, Eflornithine, Everolimus, Histrelin, Infliximab, CTSL, FURIN, TMPRSS2, ACE2, DPP4, SLC6A, MASTL, AFM, CDSN, ORF1, ORF1ab, ORF6, ORF8, ORF7a, ORF3a, ORF7b, APPS, CPSB, RECEUP, FUR, PACE, PCSK3, SPC1 ADABP, ADCP2, CD26, DPPIV, TP103 protein-ligand networks above, we observed that many small molecules, including several approved drugs, could potentially compete with other proteins for binding at interaction sites.

In Figure 4, Pipeline for the comparison of SARS-COV-2-NOS3 G894T protein-protein and AZATHIOPRINE, CHLOROQUINE, BLEOMYCIN, COLCHICINE, CYCLOSERINE, CYCLOSPORINE, EFLORNITHINE, EVEROLIMUS, HISTRELIN, INFILIXIMAB, CTSL, FURIN, TMPRSS2, ACE2, DPP4, SLC6A, MASTL, AFM, CDSN, ORF1, ORF1ab, ORF6, ORF8, ORF7a, ORF3a, ORF7b, APPS, CPSB, RECEUP, FUR, PACE, PCSK3, SPC1 ADABP, ADCP2, CD26, DPPIV, TP103 protein-ligand analyses. A General pipeline: the structures for PLs are downloaded from PDB and those for PPIs from Interactome3D. We use the BioJava library to extract to the enzyme's pocket via pi-cation intermolecular bonding with Lys711, protein-protein and protein-ligand contacts. Finally, we calculate the intersection between PPI and PLI contacts to identify the drugs that may interfere with the PPIs. Visualization and analyses with IGB/ML-Bundle pi-pi stacking with His342, and pi-alkyl interaction with Ala579: we select a gene of interest in IGB and run the plugin twice: 1) on interactome 3D, with the PPI option, 2) on PDB, with the small molecule of Azithromycin where all residues of the selected with the enzyme, particularly between the carbonyl oxygens of the pyrazinoquinoxolinedione core with DDX11D: 1653, DEAD-box helicase 1 [Homo sapiens (human)], Chromosome 2, NC_000002.12 (15591868..15631101), DBP-RB, UKVH5d 6012 the RIG-I, RIG1, RIGI, RLR-1, SGMRT2-response pathway. Purple rectangles demonstrate the quick-tip obtained by mouse-overs of the edge between select item 1654DDX3X, ID: 1654, DEAD-box helicase 3 X-linked [Homo sapiens (human)], Chromosome X, NC_000023.11 (41333308..41364472), CAP-Rf, DBX, DDX14, DDX3, HLP2, MRX102, MRXSSB300 and DDX39A, ID: 10212, DEXD-box helicase 39A [Homo sapiens (human)], and the nodes DDX38, PRP16, PRPF16, RP84 and AGS7, Hlcd, IDDM19, MDA-5, MDA5, RLR-2, SGMRT1 respectively. Most integration data are available only after the node has been queried against the databases of the Shortest path(6)::CSNK1E-TCEB2-USP52-ERC1-YWHAG-CRTC3-NEDD1 Shortest path(6)::CSNK1E-RBX1-TP53-WDR68-YWHAG-CRTC3-NEDD1, Shortest path(6)::CSNK1E-RBX1-UBC-WDR68-YWHAG-CRTC3-NEDD1, Shortest path(6)::CSNK1E-AKAP9-UBC-WDR68-YWHAG-CRTC3-NEDD1, Shortest path(6)::CSNK1E-TCEB2-UBC-WDR68-YWHAG-CRTC3-NEDD1, Shortest path(6)::CSNK1E-RBX1-APP-WDR68-YWHAG-CRTC3-NEDD1, Shortest path(6)::CSNK1E-AKAP9-RNF2-WDR68-YWHAG-CRTC3-NEDD1, Shortest path(6)::CSNK1E-RBX1-CUL4A-WDR68-YWHAG-CRTC3-NEDD1, Shortest path(6)::CSNK1E-RBX1-SMAD3-WDR68-YWHAG-CRTC3-NEDD1, Shortest path(6)::CSNK1E-RBX1-COPS6-WDR68-YWHAG-CRTC3-NEDD1, Shortest path(6)::CSNK1E-TCEB2-COPS6-

WDR68-YWHAG-CRTC3-NEDD1, Shortest path(6)::CSNK1E-RBX1-DBB1-WDR68-YWHAG-CRTC3-NEDD1, Shortest path(6)::CSNK1E-RBX1-NEDD8-WDR68-YWHAG-CRTC3-NEDD1, Shortest path(6)::CSNK1E-TCEB2-NEDD8-WDR68-YWHAG-CRTC3-NEDD1, Shortest path(6)::CSNK1E-TCEB2-EPAS1-WDR68-YWHAG-CRTC3-NEDD1, Shortest path(6)::CSNK1E-RBX1-CUL5-WDR68-YWHAG-CRTC3-NEDD1, Shortest path(6)::CSNK1E-TCEB2-CUL5-WDR68-YWHAG-CRTC3-NEDD1, Shortest path(6)::CSNK1E-RBX1-TP53-TNRC15-YWHAA-CRTC3-NEDD, Shortest path(6)::CSNK1E-AKAP9-BMI1-TNRC15-YWHAA-CRTC3-NEDD, Shortest path(6)::CSNK1E-AKAP9-TUBGCP3-TNRC15-YWHAA-CRTC3-NEDD, Shortest path(6)::CSNK1E-RBX1-UBC-TNRC15-YWHAA-CRTC3-NEDD, Shortest path(6)::CSNK1E-AKAP9-UBC-TNRC15-YWHAA-CRTC3-NEDD, Shortest path(6)::CSNK1E-TCEB2-UBC-TNRC15-YWHAA-CRTC3-NEDD1, Shortest path(6)::CSNK1E-RBX1-ELAVL1-TNRC15-YWHAA-CRTC3-NEDD, Shortest path(6)::CSNK1E-RBX1-UBC-MARK1-YWHAA-CRTC3-NEDD, Shortest path(6)::CSNK1E-AKAP9-UBC-MARK1-YWHAA-CRTC3-NEDD, Shortest path(6)::CSNK1E-TCEB2-UBC-MARK1-YWHAA-CRTC3-NEDD, Shortest path(6)::CSNK1E-RBX1-UBC-DDIT4-YWHAA-CRTC3-NEDD, Shortest path(6)::CSNK1E-AKAP9-UBC-DDIT4-YWHAA-CRTC3-NEDD, Shortest path(6)::CSNK1E-TCEB2-UBC-DDIT4-YWHAA-CRTC3-NEDD, Shortest path(6)::CSNK1E-RBX1-CUL4A-DDIT4-YWHAA-CRTC3-NEDD, Shortest path(6)::CSNK1E-RBX1-DBB1-DDIT4-YWHAA-CRTC3-NEDD1, Shortest path(6)::CSNK1E-RBX1-BTRC-DDIT4-YWHAA-CRTC3-NEDD, Shortest path(6)::CSNK1E-RBX1-TP53-EIF4E2-YWHAA-CRTC3-NEDD1, Shortest path(6)::CSNK1E-AKAP9-TUBGCP3-EIF4E2-YWHAA-CRTC3-NEDD, Shortest path(6)::CSNK1E-AKAP9-MAGED1-EIF4E2-YWHAA-CRTC3-NEDD1 Cycle(7)::ABCC1-LAT2-OAS3-ZCRB1-CYLD-ACE2-ADAM8-ABCC1, Cycle(7)::ABCC1-SSTR5-RECQL5-ZCRB1-CYLD-ACE2-ADAM8-ABCC1, Cycle(5)::ABCC1-CAMK1G-IGHA1-ACE2-ADAM8-ABCC1, Cycle(3)::ACE2-MEP1B-LAMA4-ACE2, Cycle(3)::ABCC1-PLEKHN1-MAP1A-ABCC1, Cycle(7)::ABCC1-KTI12-DNAJC13-ZCRB1-CYLD-ACE2-ADAM8-ABCC1, Cycle(5)::ACE2-PHF23-MBD4-ZCRB1-CYLD-ACE2, Cycle(5)::ACE2-SECTM1-MRPS36-ZCRB1-CYLD-ACE2, Cycle(3)::ABCC1-PRKX-DGKK-ABCC1, Cycle(5)::ABCC1-TCL1A-NEXN-ACE2-ADAM8-ABCC1, Cycle(7)::ABCC1-PKHD1-MRPL36-ZCRB1-CYLD-ACE2-ADAM8-ABCC1, Cycle(5)::ABCC1-CLDN1-PSAP-ACE2-ADAM8-ABCC1, Cycle(5)::ABCC1-VAMP5-HHIP-ACE2-ADAM8-ABCC1, Cycle(7)::ABCC1-QSEC1-PPP1R10-ZCRB1-CYLD-ACE2-ADAM8-ABCC1, Cycle(5)::ACE2-, Shortest path(6)::CSNK1E-RBX1-NFKBIA-ERC1-YWHAG-CRTC3-NEDD1, Shortest path(6)::CSNK1E-RBX1-CUL3-ERC1-YWHAG-CRTC3-NEDD1, Shortest path(6)::CSNK1E-TCEB2-CUL3-ERC1-YWHAG-CRTC3-NEDD1, Shortest path(6)::CSNK1E-RBX1-TP53-HECTD1-YWHAG-CRTC3-NEDD1, Shortest path(6)::CSNK1E-AKAP9-BMI1-HECTD1-YWHAG-CRTC3-NEDD1, Shortest path(6)::CSNK1E-AKAP9-TUBGCP3-HECTD1-YWHAG-CRTC3-NEDD1 Shortest path(6)::CSNK1E-RBX1-UBC-HECTD1-YWHAG-CRTC3-NEDD1, Shortest path(6)::CSNK1E-AKAP9-UBC-HECTD1-YWHAG-CRTC3-NEDD1, Shortest path(6)::CSNK1E-TCEB2-UBC-HECTD1-YWHAG-CRTC3-NEDD1, Shortest path(6)::CSNK1E-RBX1-HSPB1-HECTD1-YWHAG-CRTC3-NEDD1, Shortest path(6)::CSNK1E-RBX1-FBXW11-GBF1-YWHAG-CRTC3-NEDD1, Shortest path(6)::CSNK1E-RBX1-UBC-GBF1-YWHAG-CRTC3-NEDD1, Shortest path(6)::CSNK1E-AKAP9-UBC-GBF1-YWHAG-CRTC3-NEDD1, Shortest path(6)::CSNK1E-TCEB2-UBC-GBF1-YWHAG-CRTC3-NEDD1, Shortest path(6)::CSNK1E-AKAP9-PRKACB-WDR68-YWHAG-CRTC3-NEDD1, Shortest path(6)::CSNK1E-AKAP9-PRKACA-WDR68-YWHAG-CRTC3-NEDD1ZDHC19-TERT-ZCRB1-CYLD-ACE2, Cycle(5)::ABCC1-APBA1-CMA1-ACE2-ADAM8-ABCC1, Cycle(5)::ABCC1-GRIN3B-CNTF-ACE2-ADAM8-ABCC1, Cycle(3)::ACE2-CPN1-HMCN2-ACE2, Cycle(5)::ABCC1-PARD3-PDGFA-ACE2-ADAM8-ABCC1, Cycle(3)::ABCC1-CD81-CBS-ABCC1, Cycle(7)::ABCC1-TRAFD1-SYT5-ZCRB1-CYLD-ACE2-ADAM8-ABCC1, Cycle(5)::ACE2-BCAS1-BZW2-ZCRB1-CYLD-ACE2, Cycle(7)::ABCC1-UPK3A-PTGES3-ZCRB1-CYLD-ACE2-ADAM8-ABCC1, Cycle(7)::ABCC1-NEK10-THRAP3-ZCRB1-CYLD-ACE2-ADAM8-ABCC1, Cycle(3)::ACE2-IL1RL2-DPP6-ACE2, Cycle(7)::ABCC1-MMD-C21ORF2-ZCRB1-CYLD-ACE2-ADAM8-ABCC1, Cycle(3)::ABCC1-LOC731231-

UGT2B28-ABCC1AAR2, 7AAP_D, 7AAP_C, 7AAP_B, 7AAP_A, 6ZRU_A, 6ZRT_A, 7K40_A, 7K3T_A, 7K10_C, 7K10_B, 7K10_A, 7K1L_B, 7K1L_A, 7JZU_B, 7JZN_C, 7JZN_B, 7JZN_A, 7JZM_B, 7JZL_B, 7JZL_C, 7JZL_A, 7JX6_B, 7JX6_A, 7JKV_B, 7JKV_A, 7D10_A, 7CAK_C, 7CAK_B, 7CAI_A, 7CAI_C, 7CAI_B, 7CAI_A, 7A98_C, 7A98_B, 7A98_A, 6ZXN_C, 6ZXN_B, 6ZXN_A, 7A97_C, 7A97_B, 7A97_A, 7A96_C, 7A96_B, 7A96_A, 7A95_C, 7A95_B, 7A95_A, 7A94_C, 7A94_B, 7A94_A, 7A93_C, 7A93_B, 7A93_A, 7CMD_D, 7CMD_C, 7CMD_B, 7CMD_A, 7CJD_C, 7CJD_B, 7CJD_A, 7CJD_D, 6ZOK_j, 6ZOJ_j, 6XMK_B, 6XMK_A, 6Z97_C, 6Z97_B, 6Z97_A, 6YOR_A, 6YOR_E, 7JZ0_D, 7JZ0_C, 7JZ0_B, 7JZ0_A, 7JYY_D, 7JYY_C, 7JYY_B, 7JYY_A, 6XDH_A, 7JYC_A, 7JU7_A, 6X2A_C, 6X2A_B, 6X2A_A, 6WZQ_D, 6WZQ_C, 6WZQ_B, 6WZQ_A, 6WZO_D, 6WZO_C, 6WZO_B, 6WZO_A, 6WXD_B, 6WXD_A, 6WTM_B, 6WTM_A, 6WTK_A, 6WTJ_A, 6W9Q_A, 6M3M_D, 6M3M_C, 6M3M_B, 6M3M_A, 7JUN_A, 7JME_A, 7CTT_D, 7CTT_C, 7CTT_B, 7CTT_A, 7CJM_B, 7CE0_D, 7CE0_C, 7CE0_B, 7CE0_A, 7CDZ_D, 7CDZ_C, 7CDZ_B, 7CDZ_A, 7CBT_B, 7CBT_A, 7C8D_B, 7C8B_A, 7C6U_A, 7C6S_A, 7C2Y_B, 7C2Y_A, 7C2Q_B, 7C2Q_A, 6XF6_C, 6XF6_B, 6XF6_A, 6XF5_C, 6XF5_B, 6XF5_A, 6ZWV_C, 6ZWV_B, 6ZWV_A, 6XEY_C, 6XEY_B, 6XEY_A, 6XKL_C, 6XKL_B, 6XKL_A, 6XCN_E, 6XCN_C, 6XCN_A, 6XCM_C, 6XCM_B, 6XCM_A, 6XDG_E, 7C2J_B, 7C2J_A, 7C2I_B, 7C2I_A, 6WEY_A, 7JRN_J, 7JRN_A, 7JR4_A, 7JR3_A, 7JPE_B, 7JPE_A ACE2-ADAM8-ABCC1, Cycle(5)::ACE2-EMILIN3-FAM96A-ZCRB1-CYLD-ACE2, Cycle(7)::ABCC1-CDK7-CDC40-ZCRB1-CYLD-

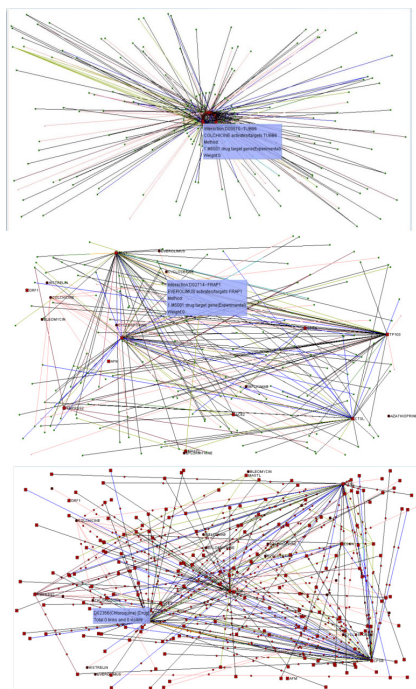


Figure 4. Pipeline for the comparison of SARS-COV-2-NOS3 G894T protein-protein and azathioprine chloroquine, bleomycin, colchicine, cyclosporine, eformithine, everolimus, histrelin, infliximab, ctsl, furin, TMPRSS2, ACE2, DPP4, SLC6A, MASTL, AFM, CDSN, ORF1, ORF1ab, ORF6, ORF8, ORF7a, ORF3a, ORF7b, APPS, CPSB, RECEUP, FUR, PACE, PCSK3, SPC1 ADABP, ADCP2, CD26, DPPIV, TP103 protein-ligand analyses.

In the list of partners of Lys711 and Arg355, we found the Cluster of the Colchicine, Baricitinib, Eformithine, Umifenofir, Hydroxychloroquine, Azathioprine, Cyclosporine and Linoleic acid Drugs which were identified during screening of a compound diversity set performed by the Biogenetoligandorol TM cluster of algorithms. The residues on the intersection track (Lys711 and Arg355/SARS-CoV2 PLpro and Lys711 and Arg355/Colchicine, Baricitinib, Eformithine, Umifenofir, Hydroxychloroquine, Azathioprine, Cyclosporine and Linoleic acid) are the Lys711 and Arg355 residues that Remdesivir shields from Hydrochloroquine. These residues are Phe19, Trp23, and Leu26, which are located in an alpha-helical region of

the SARS-CoV2 PL pro N terminus that binds to the N-terminal Lys711 and Arg355 hydrophobic pocket [17]. The scaffold of the Colchicine, Baricitinib, Eformithine, Umifenofir, Hydroxychloroquine, Azathioprine, Cyclosporine and Linoleic acid small molecules target these three critical SARS-CoV2 PLpro residues; the compound therefore competes with endogenous SARS-CoV2 PL pro for binding to Lys711 and Arg355. In the absence of a structure between Lys711 and Arg355 and SARS-CoV2 PL pro and knowing that the combination of the Colchicine, Baricitinib, Eformithine, Umifenofir, Hydroxychloroquine, Azathioprine, Cyclosporine and Linoleic acid small molecules disrupts this interaction, it would have been possible to exploit our strategy to infer some of the contact residues between Lys711 and Arg355 and SARS-CoV2 PLpro. Lys711 and Arg355 are involved in three additional interactions for which a structure is available. We created a new track to display the contacts with each of those: Lys711 and Arg355, and SARS-CoV2 PL pro. Interestingly, the Lys711 and Arg355 homo-dimerization site intersects with the Lys711 and Arg355-Colchicine, Baricitinib, Eformithine, Umifenofir, Hydroxychloroquine, Azathioprine, Cyclosporine and Linoleic acid interface, suggesting that they may also interfere with Lys711 and Arg355 homodimerization.

Conversely, the contacts that Lys711 and Arg355 makes with the cluster of the Colchicine, Baricitinib, Eformithine, Umifenofir, Hydroxychloroquine, Azathioprine, Cyclosporine and Linoleic acid drugs and SARS-CoV2 PL pro are distinct from the ones with the Colchicine small molecule: The Lys711 and Arg355/Colchicine, Baricitinib, Eformithine, Umifenofir, Hydroxychloroquine, Azathioprine, Cyclosporine and Linoleic acid and Lys711 and Arg355/SARS-CoV2 PLpro interactions may not be affected by this ligand, suggesting an edgetic effect of this compound. Our prediction that Remdesivir does not interfere with the Lys711 and Arg355/SARS-CoV2 PLpro interaction is supported by data showing that Lys711 and Arg355 and SARS-CoV2 PLpro co-immunoprecipitate following Colchicine, Baricitinib, Eformithine, Umifenofir, Hydroxychloroquine, Azathioprine, Cyclosporine and Linoleic acid treatment, which is consistent with Darunavir, Azithromycin and Linoleic acid-stimulated, Lys711 and Arg355-dependant degradation of SARS-CoV2 PL pro [28, 30].

Quantum Circuit, Binding free energy calculation and In Silico Screening Inverse Molecular Docking Algorithm

Inverse Molecular docking calculations were completed using Ligandorol TM® docking suits (Bio-genetoligandorol TM, Release 2019-1, Platform Windows-x64) using the Bio-genetoligandorol TM workflow. This workflow utilized three docking precisions, HTVS, SP, and XP, which yielded the top 10% of hits for each binding site such as the identification of conserved Arg355/SARS-CoV2 PLpro binding pockets. Both proteins were prepared by restrained minimization using force field OPLS3e. The grid sites were created using Glide® receptor grid generator with docking length of 20 Å. Grids centers were determined from active residues on target protein in order to find a pocket combination. Ligands were prepared using force field OPLS3e and possible states were generated from pH 7.0 ± 2.0. Docking scores are reported in -57.4 Kcal/mol, the more negative the number, the better binding. The surface glycoprotein (Wuhan seafood market pneumonia virus) (Sequence ID: YP_009724390.1) structure was modeled using Mod Base [29] which utilized modeller [30] for the structural modeling. The sequence (NCBI Accession: YP_009724390) was uploaded to the mod base interface and was run with the template being SARS spike protein receptor binding domain (PDB: 6XS6 SARS-CoV-2 Spike SARS-CoV-2 Main protease PDB: 6LU7 with Unliganded Active Site (2019-NCOV, Coronavirus Disease 2019, variant, minus RBD). The sequence identity was found to be 73%). The calculation was completed and imported into BiogenetoligandorolTM®. The structure was then minimized using the force field OPLS3e, the overlay of the pre and post minimized structure can be seen in Figure 2. The combination of HPC and high-efficiency platforms that enabled our country has the ability to deal with the super-high-throughput screening tasks of handling the acute infectious diseases. Selection of docking softwares Seven docking softwares were carefully evaluated to build consensus strategy, including AUTODOCK [20], VINA [21], DOCK [22], PLANTS [23], PSOVINA [24], LEDOCK (<http://www.lephar.com>) and

GOLD [25]. This selection covers a wide variety of conformation search algorithm and scoring function (Table 1), thus representing an abundant source for optimizing the Bio-genetoligandoroil TM consensus protocol. The docking calculation was performed on the prepared dataset of 195 receptors and ligands by using these seven docking softwares based on default parameters. The box within the surrounding 12.5 Å of the bound ligand was defined as active site. 100 conformations for each ligand versus its corresponding active site were produced by each software. The one with highest score were selected as the final pose.

Table 1. Total Energy (van der waals forces), Hydrogen Bond electrons and Average of eighteen different ligands in observation.

Ligand	Total Energy (Van der Waals forces)	Hydrogen Bond electrons	Average
cav6lu7_02J-Hydroxychloroquine-0.pdb	-51.6645	0	14.2609
cav6lu7_02J-Azathioprine-0.pdb	-44.9234	0	18.5263
cav6lu7_02J-Azithromycin-0.pdb	559.782	0	16.3269
cav6lu7_02J-Baricitinib-0.pdb	-56.1791	0	14.8846
cav6lu7_02J-Bleomycin-0.pdb	1619.68	0	19.3646
cav6lu7_02J-Cobicicistat-0.pdb	-3.56578	0	12.9074
cav6lu7_02J-Colchicine-0.pdb	-67.3893	0	14.2069
cav6lu7_02J-Cycloserine-0.pdb	-34.8634	0	25.8571
cav6lu7_02J-Darunavir-0.pdb	169.496	0	13.0789
cav6lu7_02J-Eflornithine-0.pdb	-38.2115	0	19
cav6lu7_02J-EIDD-2801_MK-4482-0.pdb	145.787	0	17.0435
cav6lu7_02J-GC376-0.pdb	38.1646	0	8.85294
cav6lu7_02J-Histrelin-0.pdb	2154.37	0	19.3229
cav6lu7_02J-Linoleic acid-0.pdb	-31.2701	0	18.5
cav6lu7_02J-Minocycline-0.pdb	43.9429	0	13.0303
cav6lu7_02J-Remdesivir_Gilead_-0.pdb	87.8714	0	14.2619
cav6lu7_02J-Ritonavir-0.pdb	244.512	0	14.04
cav6lu7_02J-Umifenovir-0.pdb	-56.0081	0	14.1724

In Figure 5, Quantum circuit of the Bio-genetoligandoroil TM cluster of repurposing and hope-re-targeting inverse for molecular docking algorithms. Gate nG0 (param q {hq}; qreg q(3); creg c(3); reset q(0); reset q(0); reset q(1); h q(0); u2(pi/2,pi/2) q(0); measure q(1) ->c(1); x q(0); reset q(0); reset q(1); u3(pi/2,pi/2,pi/2) q(0); measure q(1)->c(1); u2(pi/2,pi/2) q(1); cswap q(0),q(0),q(1); barrier q(0); u2(pi/2,pi/2) q(1); h q(0); t q(1); t q(0); measure q(0)->c(0); ch q(0),q(1); s q(1); crx(pi/2) q(0),q(1); cu1(pi/2) q(0),q(1); tdg q(1); sdg q(1); cy q(0),q(1); crz(pi/2) q(0),q(1); ch q(0),q(1); sdg q(0); u2(pi/2,pi/2) q(1); ry(pi/2) q(1); cu3(pi/2,pi/2,pi/2) q(0),q(1); tdg q(0); nG0(pi/2) q(1); crx(pi/2) q(0),q(1); cu1(pi/2) q(0),q(1); cswap q(0),q(0),q(1); swap q(0),q(1); cz q(0),q(1); rxx(pi/2) q(0),q(1); u1(pi/2) q(0); cry(pi/2) q(0),q(1); crz(pi/2) q(0),q(1); measure q(0) -> c(0); z q(0); measure q(0) -c(0); z q(0); rx(pi/2) q(0); rx(pi/2) q(0); u2(pi/2,pi/2) q(0); rx(pi/2) q(0); ch q(0),q(1); ry(pi/2) q(0); ch q(0),q(1); u3(pi/2,pi/2,pi/2) q(0); cz q(0),q(1); ch q(0),q(0); u1(pi/2) q(0); swap q(0),q(1); sdg q(1); V = -p+0Uatt-m+12 m | Δ |

2-12 s | Δ | 2-kBTnc ∑ i=1cie- qi/kBT-1., 18 ∂ S ∂ t'=S2x+S2ySzz+S2x+S2zSyy+S2y+S2zSxxS2x+S2y+S2zSxSySxy2SxSzSxz+2S2SySyzS2x+S2y+S2z+S2x+S2y+S2zV , 18Sn+1ijk-Snijk=(x 2x y 2y + z 2z) Snijk+fnijk; equations with spin, the existence of quantum symmetry operators, and the presence of conserved charges. In this article, we are concerned similarly, for the Euclidean vectors a and b Rn, this operation is giving by a- b, with the efficient Numerical Supercritical entanglement in this local system to the area law for quantum matter of the nn(x,y)=(0,0) (1,0) (1,1) Mn,m2 (0,0),(n,m),(2n,0)S=2 log2(s)2nπ+12 log2(2πn)+(-12)log2e bits, =s/(2s+1) n 00↔ukdk H=Π boundary+∑j=12n-1Πjj+1+∑j=12n-1Πjj+1cross, Πjj+1≡∑k=1s[|Dkj,j+1Dk|+|Ukj,j+1Uk|+|kj,j+1k|], |k[|00-lukdk| Π boundary≡∑k=1s[|dk1dk|+|uk2nuk|] Πjj+1cross≡∑k=i|ukdj,j+1ukdi| Πjj+1cross 00↔ukdi | =1M2n∑mp e2πiAp|mp, Ap M2n|= (1/ M2n)∑mpe2πiAp → limn→∞M2n≅FA()≡∫0∞fA(x)e2πixdx, [0,1] (n) (n) n H≡H+ FF≡∑i=12n∑k=1s(|dkdk|+|ukuk|), gm|F|gm≅4n+m8s(mn) k = S n i + 1jk - S ni - 1jk/2 h { S y } nij k = S nij + 1k - S nij - 1k/2 h { S z } nij k = S nij k + 1 - S nij k - 1/2 h { S x y } nij simulation of the Langevin dynamics system. The equations governing the ith atom of an N-body Langevin system are: Πjj+1≡∑k=1s[|Dkj,j+1Dk|+|Ukj,j+1Uk|+|kj,j+1k|], |k[|00-lukdk| Π boundary≡∑k=1s[|dk1dk|+|uk2nuk|] Πjj+1cross≡∑k=i|ukdj,j+1ukdi| Πjj+1cross 00↔ukdi | =1M2n∑mp e2πiAp|mp, Ap M2n|= (1/ M2n)∑mpe2πiAp → limn→∞M2n≅FA()≡∫0∞fA(x)e2πixdx, [0,1] (n) (n) n H≡H+ FF≡∑i=12n∑k=1s(|dkdk|+|ukuk|), gm|F|gm≅4n+m8s(mn). c ∑ i = 1c i e - q i / k B T - 1 = 0, 9 S = 1 - S + S m . 11 - S + 1 - S - 2 = S m , 12 ∂ S ∂ t = S (S S + V) , 19 f n i j k = { - 2 S x S y S x y + S x S z S x z + S z S y S y z S 2 x + S 2 y + S 2 z + S 2 x + S 2 y + S 2 z V } n i j k x = { S 2 y + S 2 z S 2 x + S 2 y + S 2 z } n i j k , y = { S 2 x + S 2 z S 2 x + S 2 y + S 2 z } n i j k , z = { S 2 x + S 2 y S 2 x + S 2 y + S 2 z } n i j k , 2 x S n i j k = S n i - 1 j k - 2 S n i j k + S n i + 1 j k / h 2 2 y S n i j k = S n i j - 1 k - 2 S n i j k + S n i j + 1 k / h 2 2 z S n i j k = S n i j k - 1 - 2 S n i j k + S n i j k + 1 / h 2 { S x } n i j k = S n i + 1 j + 1 k + S n i - 1 j - 1 k - S n i + 1 j - 1 k - S n i - 1 j + 1 k / 4 h 2 { S x z } S n i j k = S n i + 1 j k + 1 + S n i - 1 j k - 1 - S n i + 1 j k - 1 - S n i - 1 j k + 1 / 4 h 2 a n d { S y z } n i j k = S n i j + 1 1 + S n i j - 1 k - 1 - S n i j + 1 k - 1 - S n i j - 1 k + 1 / 4 h 2 . 1 - x 2 2 x - y 2 2 y - z 2 2 z S n + 1 i j k = 1 + x 2 2 x + y 2 2 y + z 2 2 z S n i j k + f S n i j k . 21 1 - A x 2 1 - A y 2 1 - A z 2 S n + 1 i j k = (1 + A x 2 1 + A y 2 1 + A z 2 - A x A y A z 4) S n i j k + f S n i j k , 22 A x = x 2 x , A y = y 2 y , A z = z 2 z . 23 1 - A x 2 S n + 13 i j k = 1 + A x 2 + A y + A z S n i j k + f S n i j k 24 1 - A y 2 S n + 23 i j k = S n + 13 i j k - A y

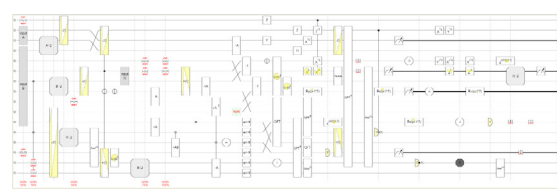


Figure 5. Quantum Circuit of the Biogenetoligandoroil TM Cluster of Repurposing and Hope-Re-targeting Inverse for molecular docking algorithms.

Before binding free energy calculation, the Sander module in Amber16 [26] program was used to perform the three-step optimization of the ligand-receptor complex. Firstly, only waters, ions and hydrogens were allowed to move. Secondly, the backbone atoms of the protein were fixed while others were allowed to move. Thirdly, all the atoms of the system were free to move. In the three optimization process, 2000 steps steepest descent method followed by 2000 steps conjugated gradient method were used for each ligand-receptor binding system. The RMSD gradient goes from dark green (for high-accuracy near-native docking solution with RMSD below 1.0 Å), to dark (RMSD ≥ 10.0 Å). A docking pose was considered as near-native pose once its backbone RMSD is ≤ 2.5 Å. Finally, the binding free energy (Gbind) is calculated by using the MM/PBSA [17,18] and X-score methods [9, 20]. As for the X-score method, it is assumed that the overall binding free energy in a protein-ligand binding process can be divided into several terms (shown in Equation 1) [21]. Here, Gvdw represents the van der Waals interaction between the receptor and the ligand; GH-bond represents the

Compound	Energy	V-S-LEU-50	V-M-GLU-166	V-S-GLU-166	V-M-LEU-167	V-M-PRO-168	V-S-PRO-168	V-M-GLN-189	V-S-GLN-189	V-M-THR-190	V-S-THR-190	V-M-ALA-191	V-S-GLN-192	V-M-GLN-192	V-S-ALA-193	V-M-VAL-3	V-S-VAL-3	V-M-LEU-4		
cav6lu7_02J-Colchicine-0.pdb	-67.4	-0.32928	-2.0362	-3.00244	-4.93533	-10.5595	-8.8959	-4.06623	-0.66481	-6.26814	-0.16543	-3.47426	-0.32816	0	-11.6613	-3.21089	-5.18264	0		
cav6lu7_02J-Baricitinib-0.pdb	-56.2	-1.31486	-2.65117	-1.99069	-0.90043	-5.14416	-6.53615	-4.58126	-3.41317	-6.44081	-0.14138	-4.21058	-0.99614	0	-6.29089	-3.22596	-5.39419	0		
cav6lu7_02J-Umifenovir-0.pdb	-56	-0.26217	-1.97983	-2.26351	-2.99982	-7.18824	-4.61248	-4.39373	-5.86357	-4.99421	-0.11964	-1.96217	-0.63077	0	-9.93394	-4.81284	-1.57475	0		
cav6lu7_02J-Hydroxychloroquine-0.pdb	-51.7	0	-0.68925	-0.5275	-1.47141	-5.52144	-9.29764	-1.36171	-0.18966	-3.77773	-0.01751	-7.88658	-6.94143	-0.0551	-4.03966	-1.95583	-2.07611	0		
cav6lu7_02J-Azathioprine-0.pdb	-44.9	0	-1.49966	-3.40695	-5.45524	-10.1445	-10.9483	-0.90063	-0.1233	-2.80028	0.003767	-2.84965	-0.66062	0	-0.56361	-0.7621	-1.22511	0		
cav6lu7_02J-Effornithine-0.pdb	-38.2	0	-0.04202	-6.55779	-5.50671	-7.79413	-5.12273	0	0	0	0	0	0	0	-3.05703	-2.60076	-5.57322	0		
cav6lu7_02J-Cycloserine-0.pdb	-34.9	0	-2.75138	-3.221	-5.60998	-6.93149	-4.86722	0	0	0	0	0	0	0	-4.14186	-2.87257	-3.20017	0		
cav6lu7_02J-Linoleic acid-0.pdb	-31.3	0	-5.24786	-10.6717	-2.81361	-4.67662	-3.5281	-3.63901	0	0	0	0	0	0	-2.00542	-6.5038	14.2499	-3.34134		
cav6lu7_02J-Cobicistat-0.pdb	-3.6	-0.10478	-0.95632	-1.43524	-4.07858	-12.3993	21.5358	-0.03648	10.2221	-4.17778	0	-7.72817	-8.1896	-0.48342	-1.09156	13.077	-3.83781	-4.51486	-0.02749	
cav6lu7_02J-GC376-0.pdb	-38.2	0	32.0454	-4.13464	20.2777	-1.17983	-0.25455	2.8209	0	0	0	0	3.79212	-0.17384	-1.02478	0	-4.87626	-5.31418	-6.40258	
cav6lu7_02J-Minocycline-0.pdb	43.9	-0.63104	-0.94372	0	-0.80504	-6.05897	-2.54805	-4.51911	-6.22801	-9.51373	0	-2.75202	-0.54655	0	62.9322	1.51941	12.8638	-0.22854		
cav6lu7_02J-Remdesivir	87.9	-8.05377	-0.89637	-0.79417	-0.9146	-2.64028	-2.93899	28.1449	51.1248	-4.42675	-5.04808	-0.56416	-0.02574	0	0.8658	3.28407	36.9551	-2.22116		
Gilead -0.pdb	145.8	-0.86935	-0.82397	0	-2.35867	7.0684	67.4093	-4.32365	-1.29479	-8.55203	-0.22782	-2.93614	-0.94717	0	95.9892	5.70418	-3.23606	-0.53266		
EIDD-2801_MK-4482-0.pdb	169.5	0	-9.40233	66.3381	-2.07622	26.8654	1.24165	1.63595	0	-1.0078	0	-0.10896	-3.38309	-5.22594	-0.18721	23.2566	1.42431	-1.3037	-0.24536	
Darunavir-0.pdb	244.5	0	0	-2.86322	0	-0.22801	1.80083	56.1117	0	-4.32065	-4.03907	-9.03176	13.2729	-7.40572	62.8047	0.264186	0	0		
Ritonavir-0.pdb	559.8	-0.05888	0	-0.83603	-4.67636	89.2267	161.555	138.597	-1.6001	-0.97197	-2.70069	0	-4.04654	5.89791	-0.57292	2.65023	10.9296	-3.0056	-3.48234	
Azithromycin-0.pdb	1619.7	16.4581	102.257	165.434	147.485	199.053	21.9155	25.2655	63.4489	-2.7567	24.3926	47.7437	-5.92753	8.70513	173.551	1.2247	-0.71966	10.1888	-1.12622	8.36343
Bleomycin-0.pdb	2154.4	230.682	54.1426	169.292	280.705	120.419	173.659	162.984	25.4566	-6.74535	159.001	17.0357	26.9283	-3.37733	-3.82499	-0.38305	70.8141	48.9867	69.6619	-1.92863
Histrelin-0.pdb																				

Table 2. Docking Energy Ranking of the Azathioprine, Azithromycin Baricitinib, Bleomycin, Cobicistat, Colchicine, Cycloserine, Darunavir, Effornithine, EIDD-2801_MK-4482, GC376, Histrelin, Linoleic acid, Minocycline, Remdesivir, Gilead, Ritonavir, Umifenovir into the cav6lu7_02J binding cavities of the amino acids of the sequences of the V-S-LEU-50, V-M-MET-165, V-M-GLU-166, V-S-GLU-166, V-M-GLU-166, V-S-GLU-166, V-M-LEU-167, V-M-PRO-168, V-S-PRO-168, V-M-GLN-189, V-S-GLN-189, V-M-THR-190, V-S-THR-190, V-M-ALA-191, V-M-GLN-192, V-S-GLN-192, V-M-ALA-193, V-M-ALA-2, V-M-VAL-3, V-S-VAL-3, V-M-LEU-4.

During simulation, the hydrogen bond interaction between Cys145SG and His41NE2 is ranging from 3.1 to 3.3 Å and the average H-bond interaction of W1 water center to His41ND1, Arg40NB, His164ND1, V-S-ARG-10, V-M-GLY-11, V-M-THR-12, V-S-THR-12, V-M-THR-13, V-M-VAL-14, V-S-VAL-14, V-M-ILE-15, V-S-ILE-15, V-M-LEU-16, V-S-LEU-16, V-M-LYS-17, V-S-LYS-17, V-M-GLU-18, V-S-GLU-18, V-M-PRO-19, V-S-PRO-19 and Asp187OD2 atoms are observed to be 3.0-3.3, 3.1-3.4, 2.8-3.4, 2.7-3.2 Å respectively (Figure 6). In classical proteases (like chymotrypsin, trypsin or elastase), the catalytic triad is made up of an acid, base and a nucleophile but in coronavirus main proteases (SARS-CoV-2 Mpro (PDB Id 6lu7), SARS-CoV Mpro (PDB Id 2zu5) and MERS-CoV Mpro (PDB Id 5wkk)) presence of water-mediated Aspartic acid residue along with base (His) and nucleophile (Cys) seem to be unique and reflecting the formation of water-mediated catalytic triad so, the occupation of W1 water center adjacent to the base (His41) and its recognition to Asp187 through Asp187OD2W1His41NE2 interaction could be an evolutionary change in the catalytic site of CoV-Mpro for Unknown reasons. During simulation, the Baricitinib, Eformithine, Colchicine small molecules interacted within binding sites of the Asp187 the V-M-CYS-20, V-S-CYS-20, V-M-PRO-21, V-S-PRO-21, V-M-SER-22, V-S-SER-22, V-M-GLY-23 LEU B 120, PHE B 210, GLY B 480»,»RIT B 602/ II binding sites V-M LEU 167, V-M PRO 168, V-S PRO 168, V-S GLU166, V-M GLU 189 amino acids with the docking energies of: -67.4 -0.329283, -2.0362 -3.00244, -4.93533, -10.5595, -8.8859, -4.05623, -0.664807,-6.26814, -0.165426, -3.47426, -0.328155, -11.6613, -3.21089, -5.18264, Baricitinib with -56.2, -1.31486, -2.65117, -1.99069, -0.900426,-5.14416, -6.53615, -4.58126, -3.41317, -6.44081, -0.141376, -4.21058, -0.996135 -6.29089, -3.22596, -5.39419. Interactions between the Umifenovir and Colchicine drugs and its CoV-Mpro-NOS3 protein and gene targets are caused by hydrogen bonds, Van der Waals force and π-π interaction, which are exerting their interactive forces within less than 4 Angstrom with the docking energies of the -56, -0.26217, -1.97983, -2.25351, -2.99982, -7.18824, -4.61248, -4.39373, -5.86357, -4.99421, -0.119644, -1.96217, -0.630774, -9.93394, -4.81284, -1.57475 to made through the sequence of the amino acids of the V-S-PHE-3 V-S-ARG-4 V-M-MET-6 V-S-MET-6 V-M-ALA-7 V-M-PHE-8 V-S-PHE-8 V-M-PRO-9 V-S-PRO-9 V-M-THR-25 V-S-ARG-40 V-S-HIS-41 V-M-THR-45 V-M-SER-46 V-S-SER-V-M-PRO-52 V-M-ASN-53 V-S-ASN-53 V-S-GLU-55 V-M-VAL-125 V-M-TYR-126 V-M-SER-139 V-M-ASN-142 V-S-ASN-142 V-M-GLY-143 V-S-CYS-V-M-MET-165 V-S-MET-165 V-M-GLU-166 V-S-GLU-166 V-M-LEU-167 V-S-VAL-186V-M-ASP-187 V-S-ASP-187 V-S-GLN-189 V-S-THR-199 V-M-PHE,-V-S-PHE-223, Asp187OD2W1His41ND1/NE2Cys145SGLEU B 120, GLY B 480»,»RIT B 602/II (O25) path. The carbonyl oxygen (O25) is stabilized by amide backbone atoms of Cys145, Ser144, and Gly143 residues where $\phi(x)$ is the new spatially varying band minimum, $V(x)$ is the externally applied potential, and $K(x, x')=K_0(x-x')^2+2\sqrt{x(t)}=Ax(t)+Bu(t)$ $x(t)=Ax(t)+Bu(t)$ $x(t)=Ax(t)+Bu(t)$ $O(NL)$ $W=[AB00]$, $x(t)=Ax(t)+Bu(t)$, $x'=Ax+Bu^*$, $M=[100010001000]$, $x'=Ax+BD^*M(MTu)$, $\min D \sum_j=1 P d_j$, $d_j=[0,1]$, $j=1,2,\dots,P$, $[G_i=[i1i2\dots ini1i2in]]$ gives the Coulomb potential between points x and x' . K_0 sets the energy scale of the interaction and $\int K(x,x')n(x)dx^i1+2+2+2+2=1, i=1,2,\dots, m, G_i=[G_i1G_i2]$, $\{G_i1=[i1, i2, \dots, ij, \dots, in] G_i2=[i1, i2, \dots, ij, \dots, in]$, $Pen(D)=\sum_i=1 IPeni(D)$, $f(D)=\sum_j=1 P d_j+Pen(D)=\sum_j=1 P d_j+\sum_i=1 Iix(rank(iin-A, BDM)-N)2$, $pen(D)=10P^*\sum_i=1 IPeni(D)=50^*1\neq 0, Q(t)=(G1t, G2t, \dots, Gmt)$, $Git=[i1ti2t\dots iPt1ti2tiPt]$, $i=1,2,\dots, m, t=0,2,\dots, maxgen-1$, gives the effective Coulomb potential created as a result of the electron density $n(x)$.

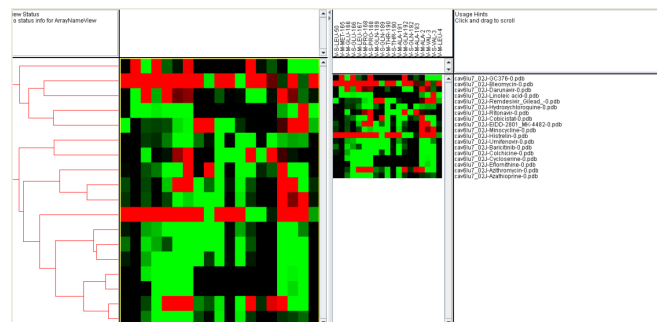


Figure 6. Cluster analysis of the docking interactions of the azathioprine, azithromycin baricitinib, bleomycin, cobicistat, colchicine, cycloserine, darunavir, eformithine, EIDD-2801_MK-4482, GC376, histrelin, linoleic acid, minocycline, remdesivir_gilead, ritonavir, umifenovir.

Discussion

The hit compounds of the Colchicine, Baricitinib, Eformithine, Umifenovir, Hydroxychloroquine, Azathioprine, Cycloserine and Linoleic acid drugs reported here have potential to inhibit the 6LU7 crystal structure of COVID-19 main protease variant but are not guaranteed to have any activity; however, this lays the groundwork for computational drug discovery for new compounds to reduce transmission and symptoms of SARS-CoV-2. We have used structural homology modeling through the use of computer, quantum mathematical, Euclidean geometrics and statistical methods to determine a dock-able target for the SARS-CoV-2 spike protein and have utilized the newly characterized SARS-CoV-2 Spike SARS-COV-2 Main protease PDB:6LU7 with Unliganded Active Site (2019-NCOV, Coronavirus Disease 2019, variant in our docking models. It is also exciting to uncover that this combination of drugs may also be potentially used for the treatment of SARS-CoV-2 infections. At this point it is important to be mentioned that the Biogenea Pharmaceuticals Ltd for Pharmaceutical Biotechnology Drug Design laboratory celebrates with people, procedures, and vision that bring new drugs into the market through Molecular Biochemistry and Molecular Pharmacology. We target the development and manufacture of new drugs like a small molecule, a nano-ligand targeted COVID-19-D614G mutation using Topology Euclidean Geometrics for Toxicity Predictive Neural Networks: A Quantum Gravitational for Persistent Homology Pharmacophoric Kinematic Algorithm (Q-Hypatia) in Practice. Such medicines draw on talent passion and experience of a wide range of professionals. The goal of Grigoriadis Ionnannis and partners is to bring this group into the limelight and, in doing so, to integrate the entire process, from the registration of an Investigational New Drug (IND) or Pharmacobiochemistry License Application (BLA) through to the market launch of new therapies and beyond. Our new computerized quantum algorithms have led us to more than one groundbreaking Pharmacobiochemical results that are to be published in the very near future time (Figures 7,8 and 9).

Compound	Energy	V-S LEU	V-M MET	V-S GLU	V-M LEU	V-S PRO	V-M PRO	V-S GLN	V-M GLN	V-S THR	V-M THR	V-S ALA	V-M ALA	V-S VAL	V-M VAL	V-S LEU	V-M LEU	
1 caifu7_021-Cyclosporine-6.pdb	-47.4	-0.3	0	-2	-3	18.8	19.8	14.9	14.7	19.2	-2.2	-1.5	-0.3	0	19.7	2.2	18.8	
2 caifu7_021-Baricitinib-6.pdb	-52	-1.3	0	-2.7	-2	-0.5	19.1	14.9	14.4	14.4	-0.1	-0.2	1	0	19.3	-3.2	18.4	
3 caifu7_021-Umifenovir-6.pdb	-56	-0.3	0	-2	-3	-3	17.2	14.6	14.4	14.9	0	-0.1	-0.6	0	19.9	14.2	11.6	
4 caifu7_021-Hydroxychloroquine-6.pdb	-51.7	0	0	-0.7	-0.5	-1.6	18.5	19.3	14	-0.2	-3.8	0	17.9	14.9	0.1	14	2.3	-2
5 caifu7_021-Azithromycin-6.pdb	-44.9	0	0	-1.5	-3.4	18.1	19.8	14.9	14.9	-0.1	-0.8	0	-2.8	-0.7	0	18.6	-1.2	-0.6
6 caifu7_021-Colchicine-6.pdb	-38.2	0	0	0	0	18.5	14.5	17.8	15.1	0	0	0	0	0	0	-3.1	-2.9	18.8
7 caifu7_021-Cycloserine-6.pdb	-34.9	0	0	-2.8	-3.2	18.8	14.9	14.9	0	0	0	0	0	0	0	14.1	-2.9	-3.2
8 caifu7_021-Linoleic acid-6.pdb	-21.3	0	0	15.2	19.7	2.9	4.7	3.5	-3.6	0	0	0	0	0	0	-2	18.2	-3.3
9 caifu7_021-Eformithine-6.pdb	-13.6	-4.1	0	-1	-1.4	14.1	16.6	17.5	0	19.2	0	0	19.7	14.2	-4.5	-1.1	15.1	-3.1
10 caifu7_021-GC376-6.pdb	38.2	0	32	14.1	20.3	-1.2	-0.3	-2.3	0	19.2	0	0	0	3.8	-0.2	-1	0	14.9
11 caifu7_021-Minocycline-6.pdb	43.9	-0.6	0	-0.9	0	-0.8	16.1	-2.5	14.5	16.2	16.5	0	-2.8	-0.5	0	16.9	15	12.9
12 caifu7_021-Remdesivir_gilead-6.pdb	87.9	0	-0.9	-0.8	-0.9	-2.9	29.1	51.1	4.9	0	0	0	0	0	0	19.9	3.3	17
13 caifu7_021-EIDD-2801_MK-4482-6.pdb	145.8	-0.9	0	-0.5	0	-2.4	11	19.4	16.8	11.3	16.2	-0.2	-2.9	-0.9	0	16	5.7	-3.2
14 caifu7_021-Darunavir-6.pdb	189.5	0	18.4	16.3	-0.1	26.9	1.2	1.6	0	0	0	-1	-0.1	-3.4	19.2	-0.2	23.3	1.4
15 caifu7_021-Ritonavir-6.pdb	244.5	0	0	-2.9	0	-0.2	1.8	56.1	0	0	0	1.3	1.4	0	13.3	14.4	10.8	-0.3
16 caifu7_021-Azithromycin-6.pdb	509.8	-0.1	0	-0.9	18.7	19.2	191.6	126.6	-1.9	-1	-2.7	0	0	0	0	19.9	-0.6	2.7
17 caifu7_021-Histrelin-6.pdb	1193.7	16.5	102.3	165.4	112.5	196.1	21.9	25.5	13.4	2.8	24.4	17.7	16.8	17	175.5	1.2	-2.7	
18 caifu7_021-Histrelin-6.pdb	2154.4	236.7	54.1	189.3	280.7	129.4	173.7	163	26.5	16.7	15.9	17	25.9	-3.4	-3.8	-0.4	70.8	49

Figure 7. 3D docking interactions of the azathioprine, azithromycin, baricitinib, bleomycin, cobicistat, colchicine, cycloserine, darunavir, eformithine, EIDD-2801_MK-4482, GC376, histrelin, linoleic acid, minocycline, remdesivir_gilead, ritonavir, umifenovir into the binding sites of the 6YB7 SARS-CoV-2 main protease PDB:6LU7 with unliganded active site (2019-nCoV, coronavirus disease 2019, COVID-19) sequence of amino acids.

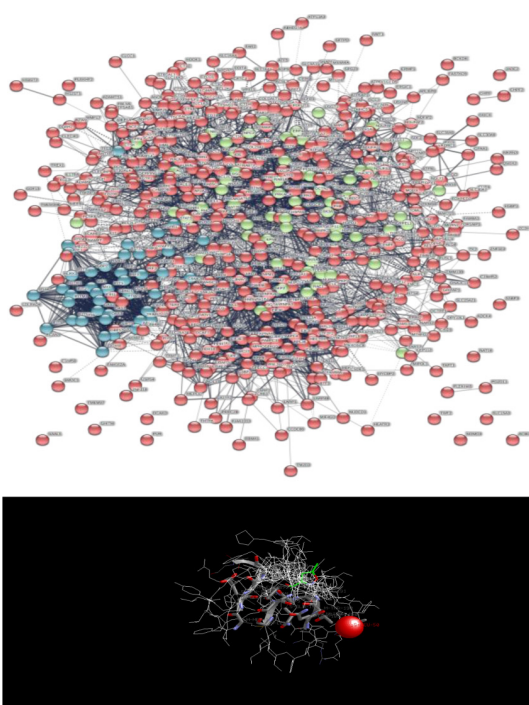


Figure 8. 3D Docking interactions of the the azathioprine, azithromycin, baricitinib, bleomycin, cobicistat, colchicine, cycloserine, darunavir, efnornithine, EIDD-2801_MK-4482, GC376, histrelin, linoleic acid, minocycline, remdesivir_gilead, ritonavir, umifenovir into the binding sites of the 6YB7 SARS-CoV-2 main protease PDB:6LU7 with unliganded active site (2019-nCoV, coronavirus disease 2019, COVID-19).

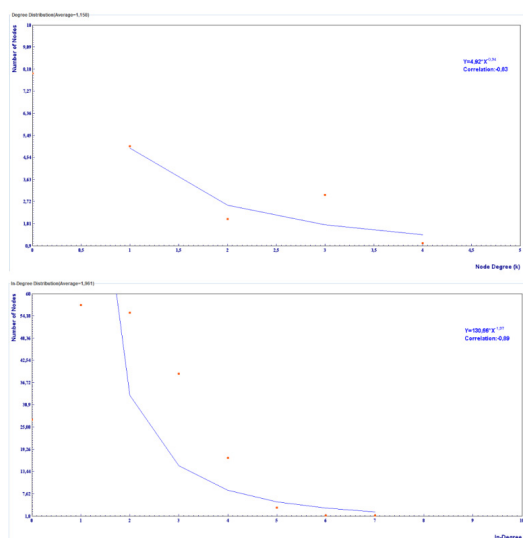


Figure 9. Clustering-coefficient distribution analysis between the cluster of the azathioprine, azithromycin baricitinib, bleomycin, cobicistat, colchicine, cycloserine, darunavir, efnornithine, EIDD-2801_MK-4482, GC376, histrelin, linoleic acid, minocycline, remdesivir_gilead, ritonavir, umifenovir small molecules (average=1,961).

Conclusion

At the end of block-buster era for drug discovery, drug repurposing is a promising approach to address the productivity gap, that the global pharmaceutical giants are currently facing, which will improve the drug-discovery productivity. In this original article we applied Inverse docking protocols with the integration of various COVID-19 disease databases, to perform data mining for the de novo drug repurposing, in the potential binding cavities of a set of clinically relevant macromolecular NOS3 targets.

The critical issues related to inverse docking part are the prediction of correct binding pose and the estimation of some measure of the binding affinity. We have evaluated of several docking methods for inverse docking applications since the effectiveness of these methods in multiple target identification is unclear. A consensus ORF1a-NOS3-Colchicine, Baricitinib, Efnornithine, Umifenovir, Hydroxychloroquine, Azathioprine, Cycloserine and Linoleic acid driven inverse docking protocol was developed, which has a~10% enhancement in success rate compared with the best single docking algorithm. Finally, an comprehensive web platform by applying AI deep learning models was designed based on our Bio-genetoligandrol TM protocol for drug repurposing to significantly reduce user time for data gathering and multi-step analysis without human intervention, which consists of the following three tools:

- An automated consensus inverse docking workflow program,
- A compound database containing 2086 approved drugs with original therapeutic information,
- A known target database containing 831 protein structures from PDB covering 30 therapeutic areas.

Differentiated with other tools, Bio-genetoligandrol TM outperforms other standalone algorithm in a better accuracy and more efficient way in summary. We anticipate that the Colchicine drug could interact synergistically with the active compounds of Umifenovir, Hydroxychloroquine, Azathioprine, baricitinib, Efnornithine, Cobicistat, Cycloserine and Linoleic acid but not with the Minocycline, Remdesivir, EIDD-2801, Darunavir, Ritonavir, Azithromycin, Bleomycin, Histrelin drugs to kill SARS-COV2 viruses.

References

1. Sun, Xiaoxuan, Yicheng Ni, and Miaojia Zhang. "Rheumatologists View on the use of Hydroxychloroquine to Treat COVID-19." *Emerg Microbes Infect* 9(2020): 830-832.
2. Maheshkumar, Kuppusamy, Wankupar Wankhar, Krishna Rao Gurugubelli, and Vidyashree Hodagatta Mahadevappa, et al. "Angiotensin Converting Enzyme 2 (ACE2): COVID 19 Gate Way to Multiple Organ Failure Syndromes." *Respir Physiol Neurobiol* 283(2020): 103548.
3. Johns, Robin, Zhao Feng Chen, Lufei Young, and Flordelis Delacruz, et al. "Meta analysis of NOS3 G894T Polymorphisms with Air Pollution on the Risk of Ischemic Heart Disease Worldwide." *Toxics* 6 (2018): 44.
4. Singh, A. "How AI is fighting COVID-19: the companies using intelligent tech to find new drugs." *Pharmaphorum* (2020).
5. Scudellari, Megan. "Five Companies Using Ai to Fight Coronavirus." *IEEE Spectrum* (2020).
6. Guilliams, T. "Healx Joins Forces with Boehringer Ingelheim to Discover New Treatment Approaches for Rare Neurological Diseases." *Healx News* (2019).
7. De Clercq, Erik. "The Design of Drugs for HIV and HCV." *Nat Rev Drug Discov* 6(2007): 1001-1018.
8. Aanouz, I, Belhassan A, El Khatabi K, and Bouachrine M, et al. "Moroccan medicinal plants as inhibitors against SARS-CoV-2 main protease: Computational investigations." *J Biomol Struct Dyn* 65(2020):515-526.
9. Friesner, Richard A, Jay L Banks, Robert B Murphy, and Thomas A Halgren, et al. "Glide: A new Approach for Rapid, Accurate Docking and Scoring. 1. Method and Assessment of Docking accuracy." *J Med Chem* 47(2004): 1739-1749.
10. Kumar, V, Dhanjal JK, Kaul SC, Wadhwa R, and Sundar D. "Withanone and caffeic acid phenethyl ester are predicted to interact with main protease PDB:6LU7(Mpro) of SARS-CoV-2 and inhibit its activity. *J Biomol Struct Dyn*.2020; 1-13.
11. Aanouz, I, A Belhassan, K ElmKhatabi, T Lakhlifi, M Elldrissi, and M Bouachrine. "Moroccan Medicinal plants as Inhibitors against SARS-CoV-2 main Protease: Computational Investigations." *J Biomol Struct Dyn* (2020): 1-9.
12. Farhat, H, Sakr GE, Kilany R. "Deep learning applications in pulmonary medical imaging: recent updates and insights on COVID-19." *Mach Vis Appl* 31(2020); 31:53

13. Joshi, Tanuja, Tushar Joshi, Hemlata Pundir, Priyanka Sharma, Shalini Mathpal, and Subhash Chandra. "Predictive Modeling by Deep Learning, Virtual Screening and Molecular Dynamics Study of Natural Compounds against SARS-CoV-2 Main Protease." *J Biomol Struct Dyn* (2020): 1-19.
14. Liu, Zhihong, Jiewen Du, Jiansong Fang, Yulong Yin, Guohuan Xu, and Liwei Xie. "DeepScreening: a Deep Learning Based Screening Web Server for Accelerating Drug Discovery." *Database* 2019 (2019): 104.
15. Sushko, Iurii, Sergii Novotarskyi, Robert Körner, and Anil Kumar Pandey et al. "Online Chemical Modeling Environment (OCHEM): Web Platform for Data Storage, Model Development and publishing of Chemical Information." *J Comput Aided Mol Des* 25 (2011): 533-554.
16. Walker, Theo, Christopher M Grulke, Diane Pozefsky, and Alexander Tropsha. "Chembench: A Cheminformatics Workbench." *Bioinformatics* 26 (2010): 3000-3001.
17. Saha, Rudra P, Manoj K Singh, Saikat Samanta, and Swarnav Bhakta, et al. "Repurposing Drugs, Ongoing Vaccine and New Therapeutic Development Initiatives Against COVID-19." *Front Pharmacol* 11 (2020): 1258.
18. Du, Lanying, Yuxian He, Yusen Zhou, and Shuwen Liu, et al. "The Spike Protein of SARS-CoV—A Target for Vaccine and Therapeutic Development." *Nat Rev Microbiol* 7(2009): 226-236.
19. Gordon, Calvin J, Egor P Tchesnokov, Joy Y Feng, and Danielle P Porter, et al. "The Antiviral Compound Remdesivir Potently Inhibits RNA Dependent RNA Polymerase from Middle East Respiratory Syndrome Coronavirus." *J Biol Chem* 295 (2020): 4773-4779.
20. Graci, Jason D, and Craig E Cameron. "Mechanisms of Action of Ribavirin against Distinct Viruses." *Rev Med Virol* 16(2006): 37-48.
21. Kraft, Colleen S., Angela L Hewlett, Scott Koepsell, and Anne M Winkler, et al. "The use of TKM-100802 and convalescent plasma in 2 patients with Ebola virus disease in the United States." *Clin Infect Dis* 61 (2015): 496-502.
22. Liu, Cynthia, Qiongqiong Zhou, Yingzhu Li, and Linda V Garner, et al. "Research And Development on Therapeutic Agents and Vaccines for COVID-19 and Related Human Coronavirus Diseases." *ACS Cent Sci* 6 (2020): 315-331.
23. Rifaioglu, Ahmet Sureyya, Heval Atas, Maria Jesus Martin, and Rengul Cetin-Atalay, et al. "Recent applications of deep learning and machine intelligence on in silico drug discovery: methods, tools and databases." *Brief Bioinform* 20(2019): 1878-1912.
24. Jing, Yankang, Yuemin Bian, Ziheng Hu, Lirong Wang, and Xiang-Qun Sean Xie. "Deep Learning for Drug Design: An Artificial Intelligence Paradigm for Drug Discovery in the Big Data Era." *AAPS J* 20 (2018): 58.
25. Ma, Chao, Lirong Wang, and Xiang Qun Xie. "GPU Accelerated Chemical Similarity Calculation For Compound Library Comparison." *J Chem Inf Model* 51(2011): 1521-1527.
26. Cova, Tânia FGG, and Alberto ACC Pais. "Deep Learning for Deep Chemistry: Optimizing the Prediction of Chemical Patterns." *Front Chem* 7 (2019): 809.
27. Lin, E, Lin CH, and Lane HY. "Relevant Applications of Generative Adversarial Networks in Drug Design and Discovery: Molecular De Novo Design, Dimensionality Reduction, and De Novo Peptide and Protein Design." *Molecules* 2020; 25(14):3250-2020.
28. Yang, Z, Papanikolaou S, Reid ACE, and Liao WK, et al. "Learning to Predict Crystal Plasticity at the Nanoscale: Deep Residual Networks and Size Effects in Uniaxial Compression Discrete Dislocation Simulations." *Sci Rep* 10(2020): 8262-2020.
29. Karimi, Mostafa, Di Wu, Zhangyang Wang, and Yang Shen. "DeepAffinity: Interpretable Deep Learning of Compound Protein Affinity through Unified Recurrent and Convolutional Neural Networks." *Bioinformatics* 35(2019): 3329-3338.
30. Liu, Huanxiang, Fang Bai, Ding Hong, and Yingying Lu, et al. "Prediction of the Antioxidant Response Elements Response of Compound by Deep Learning." *Front Chem* 7 (2019): 385.
31. Ching, Travers, Daniel S Himmelstein, Brett K Beaulieu Jones, and Alexandr A Kalinin, et al. "Opportunities and Obstacles for Deep Learning in Biology and Medicine." *J R Soc Interface* 15(2018): 20170387.

How to cite this article: Grigoriadis, John Ioannis. "Colchicine, Baricitinib, Eforinithine, Umifenofir, Hydroxychloroquine, Azathioprine, Cycloserine and Linoleic Acid to Stratify Synergistic Responses on SARS-COV-2 Main 6lu7 Protease: Quantum Mechanics Driven Applications of Artificial Deep Learning Similarities for a NOS3 Hypoxic Based Drug Retargeting Methodology to Treat COVID-19." *Clin Schizophr Relat Psychoses Spl 1*(2020). DOI: 10.3371/CSRP.GJFD.112520.